https://doi.org/10.5194/bg-2021-351
Preprint. Discussion started: 24 January 2022

Biogeosciences Discussions

Reviews and syntheses: Assessment of Biogeochemical Models in the Marine Environment

Kaltham A. Ismail, Maryam R. Al-Shehhi

Department of Civil, Infrastructure and Environmental Engineering, Khalifa University, Abu Dhabi, UAE

Correspondence to: Maryam R. Al-Shehhi (maryamr.alshehhi@ku.ac.ae)

Abstract. Marine biogeochemical models are key tools utilized to quantify numerous aspects of biogeochemistry including primary productivity, cycling of nutrients, redistribution of plankton, and variability of the carbon cycle in the ocean. These models are typically coupled to physical models with a horizontal resolution varying from few kilometers to more than 400 kilometers. Many of the existing biogeochemical models are commonly based on the NPZD model structure however, these models differ in their complexity determined by the number of state variables and the functional forms. Therefore, this review illustrates the types of the common biogeochemical models categorized based on the complexity levels and the governing equations. Then, applications of these models in several ecosystems of the world ocean are presented through a comprehensive assessment and evaluation of their performance in reproducing biogeochemical parameters such as chlorophyll-a, nutrients, as well as carbon and oxygen. In general, models based on functional group approach when coupled to high-resolution physical models show good estimates of surface nutrients such as nitrogen (N), phosphorous (P), silica (S) in global oceans with correlation coefficients (r) of ≥ 0.85, ≥ 0.9, and ≥ 0.78 respectively. Similarly, NPZD based models coupled to suitable physical models are found to accurately reproduce N, P, and oxygen (O) with coefficients of determination (R^2) around 0.9 (for N & P) and ~ > 0.9 (for O) particularly in the Indian and Pacific waters. In addition, highest performance for iron prediction in global oceans is found with r values between 0.7 and 0.86 particularly by functional group approach models. However, chlorophyll-a prediction has shown varying performances by all types of models with r ranging from 0.55 and 0.9. So, applications of biogeochemical models are dependent on the features of the ecosystem and the purpose of the study. Therefore, the functional group approach models are mainly applied to investigate biogeochemical cycles while NPZD models are mainly used for physical-biological investigation.

1 Introduction

Modelling the biogeochemistry of the ocean is essential to improve our understanding of the primary productivity, eutrophication, and nutrients variability. The formal definition of biogeochemistry is to quantify the chemical species exchanged between earth system reservoirs along with transformations in these reservoirs. Thus, biogeochemistry focuses on carbon and nutrients cycling between the living and non-living compartments of the ocean (Dutkiewicz et al., 2020). This is translated into including the inorganic nutrients, detrital matter and the explicit representation of the living components such as phytoplankton and zooplankton in the biogeochemical modelling. In addition, the importance of the ocean circulation manifests in the redistribution of organic and inorganic pools hence representation of currents, temperature, mixing, salinity and density are also an integral part of the biogeochemical models and have a great impact on the primary productivity and nutrients distribution in the oceans (Heinze and Gehlen, 2013).

https://doi.org/10.5194/bg-2021-351
Preprint. Discussion started: 24 January 2022


Biogeosciences Discussions Open Access EGU

Therefore, the developed biogeochemical models are mainly based on the classical NPZD approach developed by Fasham et al. (990) which stands for Nutrients, Phytoplankton, Zooplankton, and Detritus. These main four compartments, can be categorized into biotic (e.g. phytoplankton, zooplankton, fishes, whales) and abiotic (e.g. ammonium, nitrate, dissolved organic/inorganic carbon (DOC/DIC), particulate organic carbon (POC)) (Sarmiento et al., 1993). As for biota, phytoplankton and zooplankton are the core parts of it where phytoplankton are autotrophic organisms obtaining their energy from sunlight and can fix the carbon dioxide, and zooplankton are heterotrophic organisms obtaining their energy source by consuming other organisms. For the abiotic components, in addition to what was mentioned above, the biogeochemical models also consider the main limiting nutrient in the ocean which is primarily the Dissolved Inorganic Nitrogen termed as DIN. The other important limiting elements that are also considered include phosphate, iron and silicate (Lachkar et al., 2020). The representation of these compartments is governed by one or more state variables which can be used to define the trophic levels of the pelagic ecosystems' evolution (Heinze and Gehlen, 2013).

Several substantial biochemical parameters have been studied in various ecosystems of the global oceans using different types of biogeochemical models, these parameters include chlorophyll-a, macronutrients (nitrate, phosphate, silicate), micronutrients (Fe), carbon and oxygen cycles. Chlorophyll-a is typically used as a metric of biomass concentration instead of carbon biomass in the ocean due to its unique optical properties and it is one of the widely studied parameter in the biogeochemical modelling. The level of this parameter is affected by several basic factors including: the solar radiation intensity penetrating the water column, dissolved nutrients gradients with depth, temperature, and the mixed layer depth (Sverdrup, 1953; Wroblewski et al., 1988). Although the chlorophyll-a to carbon and nutrient ratio (Chl: C:nutrient) is highly variable due to an acclimatize response to changes in environmental conditions such as irradiance, temperature, and nutrient availability, this flexibility is neglected by many large-scale biogeochemical models for the sake of simplicity and lowering complexity (Anugerahanti et al., 2021). Whereas Macronutrients such as Nitrate (NO_3), Silicate (SiO_3), and Phosphate (PO_4) play a critical role in phytoplankton growth and ocean dynamics and these nutrients are considered to be key limiting nutrients impacting oceanic primary productivity; however, iron is recently well established to be also one of the key limiting nutrients highly impacting phytoplankton dynamics and primary productivity. These limiting nutrients can be supplied to the ocean through several sources including: dust deposition from atmosphere, riverine inputs, sea ice, sediment mobilization, as well as hydrothermal vents (Aumont et al., 2015). Unlike other nutrients, iron sources in the ocean

https://doi.org/10.5194/bg-2021-351
Preprint. Discussion started: 24 January 2022

mainly come from the atmosphere, transported as aerosols and commonly related to soil dust. Different phytoplankton groups have different sensitivity to iron limitation, for example diatoms exhibited a large sensitivity to iron limitation (Gregg et al., 2003) compared to other phytoplankton types. Likewise, carbon is the primary element in the photosynthesis process carried out by autotrophs mainly phytoplankton in the surface of the ocean. It is also the energy source for many aerobic heterotrophs and autotrophs living in the ocean. The inorganic form of carbon can be oxidized through remineralization to form inorganic sources to be utilised by photo synthesizers. While the latter convert the inorganic form back into organics for the heterotrophs. So, the atmospheric carbon dioxide is regulated by biological carbon pump which is highly impacted by the role of zooplankton in the ocean (Cavan et al., 2017). Oxygen is a by-product of photosynthesis and can be dissolved into the ocean from the atmosphere. This parameter is important for aerobic heterotrophs living in the ocean and its reduction in the ocean can lead to amplify denitrification creating oxygen minimum zone (OMZ) which is found in some regions of the global oceans (Lachkar et al., 2016, 2019, 2020).

These parameters have been modelled by several bio-geochemical models to better understand the ocean ecosystems and therefore the aim of this work is to describe the most common biogeochemical models and carry out a complete assessment of these biogeochemical models in estimating the aforementioned biochemical properties in different ecosystems. This includes reporting the performance of the models, strengths, uncertainties and limitations. This review begins with the models' section describing their components, assumptions and structure as well as examples of well-known models developed based on these approaches. Then, the major modelled parameters studied in the several ecosystems of the global oceans are discussed.

2 Biogeochemical Modelling Approaches

The existing biogeochemical models are categorized here into three types in terms of complexity, the number of state variables, and the governing equations that is formed based on the functional forms, as follow,

2.1 Classical NPZD approach

This approach basically considers a single variable for each compartment (nutrients - phytoplankton - zooplankton – detritus sometimes includes bacteria) neglecting the differences between the species (Evans et al., 1985; Fasham et al., 1990, 1993; Franks P, 2002). In this approach, nitrogen is typically considered a limiting nutrient and detritus component account for the organic matter pool which are derived from fecal materials and / non-assimilated fraction

https://doi.org/10.5194/bg-2021-351
Preprint. Discussion started: 24 January 2022


Biogeosciences Discussions Open Access EGU

of grazing by zooplankton and phytoplankton decay. This detritus is recycled through two ways which are utilization by bacteria and degradation of dissolved organic nitrogen/zooplankton assimilation (Leles et al., 2016).

The general form of NPZD is presented in equations 1-4.

$$\frac{dN}{dt} = -f(I)g(N)P + R(D)D \quad (1)$$

$$\frac{dP}{dt} = f(I)g(N)P - h(P)Z - i(P)P \quad (2)$$

$$\frac{dZ}{dt} = \gamma\, Z\, h(P) - j(Z)Z \quad (3)$$

$$\frac{dD}{dt} = i(P)P + j(Z)Z + (1-\gamma)h(P)Z - R(D)D \quad (4)$$

Five transfer equations are involved in the model including: light limitation (phytoplankton response to light/irradiance) $f(I)$; nutrient limitation (uptake of nutrients by phytoplankton) $g(N)$; grazing by zooplankton $h(P)$; loss terms due to excretion, death, and predation by other organisms $i(P)P, j(Z)Z$; degradation of detritus $R(D)$.

The zooplankton assimilation is termed as γ which is commonly modelled by a simple linear function of food ingestion (Franks P, 2002). The functional forms representation of phytoplankton response to incident light ranges from a simple linear form to nonlinear functions including saturation and photo-inhibition response (see Table 1). The Michaelis-Menten/Monod saturation function is the most applied form of nutrient uptake by phytoplankton which can relate the growth rates to the concentration of a limiting nutrient (Dugdale, 1967). The dependency of the growth on nutrient concentration is regulated by two kinetic parameters which represent the population traits: the maximum utilization rate, V_{max} ; and the affinity constant, k, which presents an organism ability to capture nutrient ions at low nutrient concentration N. The phytoplankton acclimation determines the ability of the cell to adapt its kinetic parameters in response to changes in environmental conditions. So, if V_{max} is constant then the acclimation will be discarded in the Michaelis-Menten formulation because the maximum uptake rate is associated with the total number of uptake sites of the cell (Bonachela et al., 2015). However, the Michaelis-Menten assumption was argued by (Droop, 1973, 1983) which has assumed that the growth rate is more likely dependent on the internal content of the nutrients than the external concentration showing luxury uptake of nutrients (utilization of non-limiting nutrient exceeding the level required for growth) (Cherif and Loreau, 2010). Hence, the growth of phytoplankton is described by a function of internal concentration (Quota model), as shown in Table 2. In addition, it is argued that the growth rate is determined

https://doi.org/10.5194/bg-2021-351
Preprint. Discussion started: 24 January 2022

by the most limiting process either photosynthesis or nutrient uptake permitting for switching between the two limiting processes based on the conditions (Franks P, 2002). Whereas zooplankton functional response is typically modelled with a simple functional form represented by (HOLLING CS, 1959): Holling Type I with linear function, Holling Type II with hyperbolic curve like Monod function accounting for saturation; and Holling Type III accounting for saturation and switching when the prey is low in density (sigmoidal). The zooplankton is considered as the closure term in plankton models and the zooplankton grazing functional forms impact model outputs greatly. For example, high oscillations of the states over time (destabilization effect) are determined using type II while steady state (stability) is easily obtained with type III and no impact on model stability was determined with type I. Phytoplankton and zooplankton mortality functions ranges from linear to non-linear forms (Tables 3 and 4).

Modifications have been also made in the NPZD approaches such as by replacing the bacteria compartment with chlorophyll-a to enhance the estimation of nitrogen flux (Fennel et al., 2006) and introducing a nitrogen based nutrient-phytoplankton-heterotroph model which is of intermediate complexity with respect to Fasham & McGillicuddy models (Fasham et al., 1990; McGillicuddy et al., 1995). The number of compartments has also been increased including more variables (plankton species as well as nutrients) as seen in Chai and Leonard models which are based on five and nine compartments NPZD models respectively (Chai et al., 1996; Leonard et al., 1999). Nevertheless, Galbraith et al. (2009) has developed a model based on NPZD but with Light Iron Nutrients and Gasses called BLING model, This model can isolate the global impact of iron on maximum light-saturated photosynthesis rates from photosynthetic efficiency. It considers an implicit representation of phytoplankton which is determined from the growth rate of phytoplankton. The iron representation doesn't rely on Liebig law of the minimum that is typical in the biogeochemical models, however, the nutrient-light co-limitation is incorporated in accordance with field and laboratory measurements of phytoplankton. There have been other extensions of the classical NPZD which have been applied regionally in (Doney et al., 1996; Fennel et al., 2001; Hinckley et al., 2009; Hood et al., 2003; Kearney et al., 2020; McCreary et al., 1996; McCreary et al., 2001).

2.2 Carbon cycle-based approach

In this approach, the marine biota model is introduced into a full ocean carbon cycle model to study the impact of biology on the oceanic carbon cycle. The carbon cycle model typically includes dissolved inorganic carbon and total alkalinity components. An example of this approach is the Hamburg model of the oceanic carbon cycle (HAMOCC)

https://doi.org/10.5194/bg-2021-351
Preprint. Discussion started: 24 January 2022

146 developed by (Maier-Reimer and Hasselmann, 1987) which is a pure inorganic carbon cycle model and was utilised
147 to evaluate both the 12C cycle and the ocean model residence time properties. The model neglects biological sources
148 and sinks. Therefore, it has been used as a reference for numerical experiments interpretation with extensions
149 performed by (Bacastow and Maier-Reimer, 1990; Heinze and Maier-Reimer, 1991; Maier-Reimer, 1993) to include
150 the marine biota and ecosystem processes. Bacastow & Maier-Reimer (1990) has included the first order
151 representation of the ocean plankton impacts on the ocean global inorganic oceanic carbon cycle model. While the
152 first ocean carbon cycle model featuring the representation of marine ecosystem explicitly was given by (Six and
153 Maier-Reimer, 1996). This latter is based on an extended NPZD model which includes five compartments: single
154 phytoplankton, single zooplankton, detritus, dissolved organic carbon (DOC), and single nutrient (phosphate).
155 Equations 5-11 represent the rate of change of nutrients as an example of the carbon components including: DOC and
156 particulate organic carbon (POC) embedded in the plankton model as described by (Six and Maier-Reimer, 1996).

157
$$R_{\mathrm{C:P}}\frac{\mathrm{d}N}{\mathrm{d}t} = -phytoplankton\ growth + remineralisation\ from\ herbivores + \text{remineralisation from carnivores} + DOC\ degradation + POC\ remineralisation \quad (5)$$

158 where $R_{\mathrm{C:P}}$ represents the Redfield ratio of carbon to phosphate. Whereas phytoplankton and zooplankton are
159 described as follows:

160
$$\frac{\mathrm{d}P}{\mathrm{d}t} = phytoplankton\ growth - loss\ due\ to\ grazing - natural\ decay - \text{exudation of DOC} \quad (6)$$

161
$$\frac{\mathrm{d}Z}{\mathrm{d}t} = zooplankton\ growth - loss\ due\ to\ grazing\ by\ carnivores - DOC\ excretion \quad (7)$$

162 Then, the carbon components (DOC & POC) are modelled as follows:

163
$$\frac{\mathrm{d}DOC}{\mathrm{d}t} = \gamma_P(P - P_{min}) + \gamma_Z(Z - Z_{min}) - r_{\mathrm{doc}}(N)DOC \quad (8)$$

164 where the first term represents the DOC exudation from phytoplankton; the second term represents the DOC excretion
165 from zooplankton; and the last term represents DOC degradation.

https://doi.org/10.5194/bg-2021-351
Preprint. Discussion started: 24 January 2022

$$\frac{dPOC}{dt} = F(X) - l(O_2) \quad (9)$$

where $l(O_2)$ represents remineralization of POC (for X = $(d_p, d_z, \epsilon_{her}, \epsilon_{can}, P, Z, z)$ and F(X) is the flux of dead organic carbon to the ocean interior

$F(X) = 0$; for $0 < z < 100\text{m}$

Otherwise

$$F(X) = \text{TPP}\frac{\partial}{\partial z}\left(\frac{z}{100m}\right)^{-0.8} \quad (10)$$

Where TPP is the total particle production including the particles from natural decay as well as fecal pellet production in the euphotic zone:

$$\text{TPP} = \int_0^{100\text{m}} \big((1 - \text{ zinges})(1 - \epsilon_{her})\, growth\ of\ zooplankton + phytoplankton\ mortality + (1 - \epsilon_{can})\, zooplankton\ mortality\big) \quad (11)$$

Parameter	Symbol
Mortality rate of phytoplankton	d_p
Mortality rate of zooplankton	d_z
Ingestion as fecal pellets from herbivores	ϵ_{her}
Ingestion as fecal pellets from carnivores	ϵ_{can}
Assimilation efficiency	zinges
Phytoplankton	P
Zooplankton	Z
Nutrient	N
Depth	z

The Hadley Centre Ocean Carbon Cycle (HadOCC) model is another example of Carbon cycle-based approach that is initially developed for global ocean carbon cycle modelling studies (Cox et al., 2000). The model simulates the important aspects of carbonate chemistry, the export and production of biology. Several tracers are included to model the carbon cycle including dissolved inorganic carbon, total alkalinity, single nutrient (nitrogen), oxygen, single phytoplankton, single zooplankton, as well as detritus (Palmer and Totterdell, 2001).

https://doi.org/10.5194/bg-2021-351
Preprint. Discussion started: 24 January 2022

2.3 Phytoplankton Functional group approach (PFT)

This approach includes different plankton functional types (PFTs) making it the most intricate model with at least 15 state variables relative to the other model approaches (Gregg, 2000; Gregg et al., 2003; Moore et al., 2004; Le Quéré et al., 2005). The major plankton functional types include mesozooplankton, protozooplankton, diatoms (phytoplankton silicifiers), phaeocystis, nitrogen fixers, coccolithophores, picoheterotrophs and each of these groups function differently in terms of their roles in biogeochemical cycles (Hood et al., 2006). These functional traits that reflect the functions and biochemical pathways are defined by how the cell uses energy and nutrients. The classical NPZD doesn't consider these functional types in which the aggregation of taxonomic and functional organisms in ocean ecosystems is only considered. Therefore, in the PFTs based approach, species are grouped based on their common ecological and biogeochemical functions (Hood et al., 2006; Le Quéré et al., 2005). Equations 12-14 present the general form of this approach where several phytoplankton types P_j are nourished by various nutrients N_i and grazed by many zooplankton types Z_{ki} as follow,

$$\frac{dN_i}{dt} = -\sum_j \left[\mu_j P_j M_{ij}\right] + S_{N_i} \quad (12)$$

$$\frac{dP_j}{dt} = \mu_j P_j - m_j^P P_j - \sum_k \left[g_{jk} Z_{k,i=1}\right] - \frac{\partial\left(w_j^P P_j\right)}{\partial z} \quad (13)$$

$$\frac{dZ_{ki}}{dt} = Z_{ki} \sum_j \left[\zeta_{jk} g_{jk} M_{ij}\right] - m_k^Z Z_{ki} \quad (14)$$

Parameter	Symbol
Growth rate of phytoplankton j	μ_j
Matrix of the ratio of element i to currency (which can be phosphorous, nitrogen, etc.)	M_{ij}
Sources of tracer $\boldsymbol{N_i}$	S_{N_i}
Rate of mortality/excretion of phytoplankton j	m_j^P
Grazing of zooplankton k on phytoplankton j	g_{jk}
Sinking rate for phytoplankton j	w_j^P
Grazing efficiency of zooplankton k on phytoplankton j	ζ_{jk}
Rate of mortality/excretion of zooplankton k	m_k^Z

https://doi.org/10.5194/bg-2021-351
Preprint. Discussion started: 24 January 2022

The common PFTs' models include the European Regional Seas Ecosystem Model versions (1 & 2) : ERSEM I, ERSEM II (Baretta-Bekker et al., 1997; Baretta et al., 1995; Blackford et al., 2004) which are based on a generic lower trophic approach developed to study the cycling of carbon as well as nutrients. In ERSEM, the ecosystem is divided into three functional types in which the biotic groups are classified by their functional role not by species. For instance, phytoplankton as producers; bacteria as decomposers; zooplankton as consumers which are further subdivided based on trait-size and uptake of silica to represent a food web. The functional group dynamics are represented by including population processes such as growth, migration, and mortality as well as physiological processes such as ingestion, respiration, excretion, and egestion. The phytoplankton groups involve pico-phytoplankton, nano-phytoplankton, diatoms, and non-siliceous macro-phytoplankton, while zooplankton groups include micro-zooplankton, heterotrophic nano-flagellates, and meso-zooplankton. The ERSEM model was initially applied to the North Sea to study the seasonal cycling of nutrients (N, P, S, C). A further modification has been made to the ERSEM to produce another version called Biogeochemical Flux Model (BFM). This latter accounts for the Chemical Functional Families (CFFs) in the state variables. The CFFs is split into living, non-living, and inorganic states (Vichi et al., 2007).

The Pelagic Interactions Scheme for Carbon and Ecosystem Studies (PISCES) model is another example of PFTs based model that is a modified version of HAMOCC considering 24 state variables including NO_3, NH_4, PO_4, SiO_2, Fe; small phytoplankton, large phytoplankton, small zooplankton, large zooplankton, DOM, small detritus, and large detritus (O. Aumont et al., 2003). PISCES model has been extensively used to study several ecosystems and widely applied in more than hundred studies that are based on this approach either directly or indirectly (Aumont et al., 2015). Likewise, the NASA Ocean Biogeochemical Model (NOBM) is another type of PFTs based model originally coupled to the Ocean-Atmosphere Spectral Irradiance Model (OASIM) (Gregg, 2001; Gregg et al., 2009). NOBM comprises of four phytoplankton groups, four nutrient groups (nitrate, regenerated ammonium, silica, and iron), a single zooplankton group, and three detrital pools (organic material storage, sinking, and remineralization) (Gregg, 2000; Das et al., 2019; Gregg et al., 2003; Gregg and Casey, 2007; Trull et al., 2018) (Gregg, 2001) (Gregg et al., 2003). Additionally, the PlankTOM biogeochemical model is a dynamic ocean model describing lower trophic level of marine ecosystems. This model has several extensions through varying in the number of PFTs resolved. For example, six PFTs: diatoms, coccolithophores, mixed phytoplankton, bacteria, protozooplankton and meso-zooplankton are included in PlankTOM6 (Le Quéré et al., 2005). However, additional PFTs such as nitrogen fixers, Phaeocystis, picophytoplankton and macro-zooplankton are added into PlankTOM10 (Buitenhuis et al., 2013) to evaluate the

https://doi.org/10.5194/bg-2021-351
Preprint. Discussion started: 24 January 2022

interactions between climate and ocean biogeochemistry with the wide use of data synthesis for parametrizations of the PFTs growth rates (Kwiatkowski et al., 2014) .PlankTOM resolves the cycle of carbon (C), nitrogen (N), oxygen (O), phosphorous (P), Silicon (Si), iron (Fe) cycle, three types of organic detritus, air sea fluxes of CO2, O2, Dimethyl sulphide (DMS) and N2O.

Moreover, the Model of Ecosystem Dynamics, nutrient Utilization, Sequestration and Acidification (MEDUSA) is developed by (Yool et al., 2011, 2013) is a model of intermediate complexity, constructed beyond the standard NPZD formulations. The biogeochemical cycles of iron, silicon, and nitrogen as well as small and large plankton size classes are included in this model. In this specific model, an explicit representation of internal chlorophyll quotas is included to allow for light acclimation. The key focus of MEDUSA is the biological sequestration of carbon in the deep ocean. The model is developed to study the biogeochemical response particularly of the so-called biological pump to human-induced driven change in the global ocean. Nevertheless, the tracers of phytoplankton with allometric zooplankton (TOPAZ) model is based on the interactions between the biogeochemical and the carbon cycles including two dissolved organic matter forms, dissolved inorganic species for coupled carbon (C), nitorgen (N), Phosphorous (P), Silica (S), Iron (Fe), calcium carbonate (CaCO3), dissolved oxygen (O2) heterotroph, lithogenic cycling. Additionally, processes such as gas exchange, scavenging, atmospheric deposition, denitrification and nitrogen fixation, sediment processes, and river inputs were included (Dunne et al., 2010). This model has been implemented in several studies such as (Bronselaer et al., 2020; Jung, et al., 2019; Sharada et al., 2020). The extended version of TOPAZ is the Carbon, Ocean Biogeochemistry and Lower Trophics (COBALT) which was developed to improve the planktonic food web dynamics resolution to examine the influence of climate on the flow of energy from phytoplankton to fish (Stock et al., 2014). The planktonic food web representation in TOPAZ is highly idealized including an implicit representation of zooplankton and bacteria hence, an implicit modelling of the impacts of these groups on phytoplankton and biogeochemical processes were applied. Therefore, these limitations were addressed in COBALT by including three explicit zooplankton groups, bacteria with a mechanistic parametrizations of the impacts of these groups on biogeochemistry (Stock et al., 2014b). COBALT has resolved the global scale cycles of nitrogen, carbon, phosphate, silicate, iron, calcium carbonate, oxygen and lithogenic material where small and large phytoplankton are involved. Nevertheless, DARWIN biogeochemical model is a more complex PFTs based model consisting of 78 phytoplankton types, heterotrophs, organic and inorganic forms of nitrogen, phosphorous, iron, and silica. This model was developed first to study the phytoplankton distribution especially for the cyanobacterium Prochlorococcus species

https://doi.org/10.5194/bg-2021-351
Preprint. Discussion started: 24 January 2022

by (Follows et al., 2007). The model was coupled with the general circulation model in (Wunsch and Heimbach, 2007) and was initially applied for the global distributions of phytoplankton and physiological traits. It has been applied in a followed study which has considered more biogeochemical components and enhancement of optical properties (Dutkiewicz et al., 2015; Lo et al., 2019). Nonetheless, Regulated ecosystem model (REcoM) based on functional group approach (two phytoplankton group: diatoms and nanophytoplankton; one class of zooplankton) is based on the Quota model in which the internal phytoplankton cells stoichiometry is affected by the conditions of temperature, light, and nutrients (Schourup-Kristensen et al., 2014). REcoM has also been commonly used in the Southern Ocean studies (Hauck and Völker, 2015; Losch et al., 2014; Taylor et al., 2013).

The complexity of the aforementioned PFTs models depends on number of the independent elements along with the number of PFTs considered. As regards the PFTs, simple models include one PFT which is of single phytoplankton and single zooplankton such as in HadOCC (Palmer and Totterdell, 2001). Simple models can also include two to three PFTs such as MEDUSA (Yool et al., 2013) and PISCES (Aumont et al., 2015). However, as the number of PFTs increases, the complexity of the model increases as well. As for the average elemental composition of particulate matter, it is constrained in the sea despite of the variations in the carbon to chlorophyll (C/Chl) ratios (Anugerahanti et al., 2021). The commonly used average proportion of the main elements in phytoplankton is: 106 C (carbon): 16 N (nitrogen): 1 P (phosphorous) (by atoms) and these proportionalities are termed as Redfield ratios (Redfield, 1933). Generally, adding complexity to the model doesn't necessarily improve the model skill, as has been proven in several studies which compare models with different complexities (Friedrichs et al., 2007; Kriest et al., 2010; Kwiatkowski et al., 2014; Ward et al., 2013; Xiao and Friedrichs, 2014).

3 Determination of the biochemical parameters

The aforementioned models have been applied to resolve the biochemical properties including Chlorophyll-a, Macronutrients (N,P,S), Micronutrients (Fe), Carbon and Oxygen in different ecosystems. Detailed assessments of the capabilities of these models are provided here and summarized in Table 5,

3.1 Chlorophyll-a

Chlorophyll-a concentrations have been determined using the models described above, however, the PFTs based models are found to offer more accurate estimates of Chlorophyll-a concentrations by distinguishing the

https://doi.org/10.5194/bg-2021-351
Preprint. Discussion started: 24 January 2022

283 phytoplankton types. The PFT based model PlankTOM, for instance, was used to evaluate the role of grazing versus
284 iron limitation in the low chlorophyll content (HNLC) areas of the Southern Ocean (Le Quéré et al., 2016). The
285 PlankTOM was able to produce reasonable surface chlorophyll-a estimates with correlation coefficient (r) around 0.8
286 especially in the summer season when the macro-zooplankton grazing was explicitly involved. PlankTOM5.3 has
287 shown large improvements of the interannual variation of surface chlorophyll-a relative to PlankTOM5.2 in the global
288 oceans (with residual sum of squares RSS = -13%) (Buitenhuis et al., 2013) by including a new photosynthesis
289 formulation with a representation of iron-light colimitation (Geider et al., 1998) in their fixed stoichiometry model.
290 PlankTOM10 was also compared to PlankTOM6 and applied in the Southern Ocean (Le Quéré et al., 2016). This new
291 version has similar formulations to the previous versions of the model except that it included more phytoplankton
292 groups. Both models exhibit similar results for the surface chlorophyll-a concentrations (r ~ 0.8), primary and export
293 production except that PlankTOM6 was unable to reproduce the observed low chlorophyll-a contents in summer
294 season in the Southern Ocean due to slightly deeper mixed-layer depth in the summertime. Overall, PlankTOM10 has
295 shown slightly better performance than PlankTOM6 in terms of surface chlorophyll-a distribution (bias% = 1.2%),
296 whereas the distribution of surface nutrients has been slightly lower by 5% and 2.5% for nitrogen and silica (except
297 for phosphate which shows similar performance r ~0.9). Other PFTs based models including ERSEM, DARWIN,
298 TOPAZ, PISCES, BLING and NOBM have been applied to study chlorophyll-a distribution in the surface and deep
299 oceans. ERSEM has been applied to study chlorophyll-a dynamics in the Mediterranean and has shown good r value
300 of 0.64 for the spatial distribution of the simulated and observed chlorophyll-a. However, a relatively larger bias with
301 root mean square difference (RMSD) of 0.78 was obtained for the annual mean spatial variability due to the absence
302 of cyclonic gyres of the Rhodes and South Adriatic causing intermittent blooms. In addition, the PFTs based model
303 DARWIN coupled with MITgcm in (Dutkiewicz et al., 2015) apprehended large spatial variability in chlorophyll-a
304 for the global oceans with low r around 0.55 and have shown overestimation in particularly the Southern Ocean and
305 higher latitudes. DARWIN was customized to study phytoplankton distribution in the Southern Ocean (Lo et al.,
306 2019) which has included the abundance of coccolithophores which was improved through increasing the affinity for
307 nutrients as well as coccolithophores grazing control. Two distinct size classes of diatoms (small & large) were added,
308 and two different life stages were considered for Phaeocystis (single cell vs colonial). The improvements have
309 increased the agreement between the simulated coccolithophores and diatoms with the in-situ data. However, the
310 model inaccurately has simulated diatoms and haptophytes in the Ross Sea and has overestimated the small non-

https://doi.org/10.5194/bg-2021-351
Preprint. Discussion started: 24 January 2022

311 silicified phytoplankton with general mean absolute error for diatoms and haptophytes are 0.74 mg m^{-3} and 0.22 mg
312 m^{-3} respectively. This inconsistency can be attributed to inaccuracy in representing PFT phenology and distribution.
313 Representation of co-existence within coccolithophores and Phaeocystis remains a challenge and any small changes
314 in DARWIN physiological parameters led to either Phaeocystis or coccolithophores loss. In addition, the sea-ice algae
315 representation has not been explicitly represented which may not work well in region where ice exists.

316 Concentrated Chlorophyll-a condition (i.e., Phytoplankton blooms) was also captured in the middle latitudes of the
317 Northern and Southern Hemispheres as well as in the tropical Pacific by both models (NEMO-TOPAZ and NEMO-
318 PISCES) indicating El Niño-Southern Oscillation (ENSO) condition. Both models showed an overall r between 0.6-
319 0.9 across all oceans. While the zonal averaged Chlorophyll-a was overpredicted (by ~67%) from 30°N to 45°N in
320 both models especially in the Pacific Ocean east of Japan which is due to mainly an error in the Kuroshio Current path
321 seen in low resolution models (Jung et al., 2019a). The physical model NEMO has simulated a relatively thicker mixed
322 layer which in turn simulated bigger spring blooms in this area creating a positive bias in Chlorophyll-a values in the
323 mid-latitudes of the Northern Hemispheres in biogeochemical models.

324 In contrast, underestimation of surface Chlorophyll-a in the equatorial Atlantic Ocean (bias ~-0.2 μg kg^{-1}) and the
325 Arabian Sea (bias ~-0.4 μg kg^{-1}) was also found in both models and these two areas encountering mesoscale and sub-
326 mesoscale processes impacting the biogeochemistry. NEMO-PISCES with the use of higher resolution grid than the
327 one used in (Jung et al., 2019a) presented better Chlorophyll-a distribution in the Arabian Sea with an average value
328 of ~1.3 mg Chl m^{-3} d (Koné et al., 2009). Although both models overpredicted the surface chlorophyll-a in the
329 Southern and topical Pacific (STD ~0.26 μg kg^{-1}), the NEMO-TOPAZ showed a larger bias over the equator (STD ~
330 0.22 μg kg^{-1}) for the surface Chlorophyll-a than PISCES-NEMO which is proved to be caused by the high atmospheric
331 iron deposition in TOPAZ, which is then replaced with PISCES data resulting in lowering the bias for surface
332 Chlorophyll-a. Hence, sensitivity experiments on atmospheric iron deposition can be a good task to improve the
333 surface chlorophyll-a distributions in simulations.

334 Similarly, the PFTs based model NOBM was able to predict surface Chlorophyll-a level ($r > 0.7$) in global oceans
335 (Gregg et al., 2003). However, the correct species abundance was not well identified by the model due to disparities
336 between the model and observations in particular the Indian Ocean where the observations were mainly concentrated
337 in the Arabian Sea (the model is modestly dominated by diatoms whereas observations are dominated by

https://doi.org/10.5194/bg-2021-351
Preprint. Discussion started: 24 January 2022

cyanobacteria). This might have caused by the strong upwelling in the model thus increasing nutrients concentrations which trigger faster growing organisms such as diatoms.

Nevertheless, BLING-NEMO coupled model was used to study the high Chlorophyll-a levels (i.e. blooms) (Castro de la Guardia et al., 2019) in which the spring bloom in the Barents Sea (BS) was underestimated by 1.7 mg chl m-3 while the autumn bloom underpredicted by 0.7 mg chl m^{-3}. This deviation might be attributed to the lack of nutrients from riverine input by the BLING-NEMO coupled model. Whereas the concentration representing the spring and autumn bloom in the Labrador Sea (LS) has shown an agreement with the observed seasonality, which is comparable to that of the satellite data. However, the Chlorophyll-a content is slightly overestimated by 0.2 mg chl m^{-3} during February-April due to an earlier start of the spring bloom in the simulation. Furthermore, the BLING-NEMO model has mistakenly predicted the spring blooms in March instead of April in the Hudson Bay (HB) and Baffin Bay (BB). In these two bays, the spring bloom was slightly overpredicted by 0.5 mg chl m^{-3} and ~ 0.3 mg chl m^{-3} in the BB and HB respectively. This discrepancy might be attributed to the underprediction of sea ice concentration.

Chlorophyll-a has been also derived by the carbon cycle and simple NPZD models. For example, the carbon cycle based model: HAMOCC5 was able to reproduce Chlorophyll-a with a value of 0.05 mg Ch m-3 in the oligotrophic subtropical gyres (Aumont et al., 2003) with a bias of 0.24 mg chl m^{-3}. Unlike the earlier version of the model (HAMOCC3.1) which has shown a higher concentrations of Chlorophyll-a compared to observation in these regions (Six and Maier-Reimer, 1996). This version of HAMOCC5 is an extension of HAMOCC3.1 (Six and Maier-Reimer, 1996) with the inclusion of iron and silicate limitation along with the phosphate. HAMOCC5 with its coarse resolution cannot resolve the coastal upwellings in productive regions such as Peru upwelling. The improvement of the HAMOCC was mainly in making the Chl: C ratio variable which is decreasing in the centre of the subtropical gyres to values about 1:150 while in HAMOCC3.1 this ratio remained constant at 1:60. Therefore, this model with this improvement as well as iron and silicate limiting nutrients inclusion improved the representation of chlorophyll-a content in subtropical gyres (around 0.2-0.25 mg m^{-3}).

As for the simple NPZD models, they have shown a better representation of chlorophyll-a when coupled to a high-resolution physical model as well as including correct physics representations. For example, the involvement of tides in ROMS in (Fennel et al., 2008) has improved the chlorophyll-a representations over Georges Bank which was not

https://doi.org/10.5194/bg-2021-351
Preprint. Discussion started: 24 January 2022

365 presented in the previous model (Fennel et al., 2006). The same model of (Fennel et al., 2008) was improved by adding
366 dissolved organic matter (DOM) module along with the other model components (Druon et al., 2010) to study the
367 DOM dynamics in the Northeastern U.S. continental shelves which showed a well agreement of high chlorophyll-a
368 concentrations with the satellite data particularly in the inner shelf and on Georges Bank as a result of the tidal mixing
369 and continuous nutrient supply (Bias: chlorophyll-a (with DOM) = 4 mg chl m^{-3}, chlorophyll-a (without DOM) = 6
370 mg chl m^{-3}).

371 **3.2 Macronutrients (N, P, S)**
372

373 Nutrients such as nitrate, phosphorous, and silica have been well represented by several biogeochemical models
374 (Aumont et al., 2015; Das et al., 2019; Dutkiewicz et al., 2015; Jung et al., 2019b; Lachkar et al., 2019; Pant et al.,
375 2018; Le Quéré et al., 2016; Sankar et al., 2018). The PFTs based models such as PISCES-NEMO, DARWIN-
376 MITgcm, and TOPAZ-NEMO have shown well representation of surface nutrients distribution in the global oceans
377 with r (> 0.9 for P and N; ~0.85 for S), > 0.9 for all nutrients, and > 0.95 for all nutrients respectively. Both TOPAZ
378 and PISCES have represented: (i) similar distribution of nutrients over global oceans, (ii) an overestimation in the
379 Southern Pacific Ocean bias of ≥ 4.5 μmol kg^{-1}, ~0.32 μmol kg^{-1}, and ≥ 16 μmol kg^{-1} for nitrate, phosphate, and
380 silicate respectively , (iii) higher positive bias of nitrate (≥ 0.16 μmol kg^{-1}) and silicate (≥ 8 μmol kg^{-1}) in the central
381 and southern Pacific, and the Southern Ocean and (iv) underprediction of phosphate (bias ~-0.8 μmol kg^{-1}) at the
382 middle and higher latitudes in the Northern Hemisphere (Jung et al., 2019). The discrepancies in both models can be
383 attributed to the low resolution, weak North Atlantic deep waters, and strong ventilation in the Antarctica waters.
384 However, the improvement of the optical constituents by increasing the absorption of the optical constituents resulting
385 in a reduction in the size of oligotrophic regions in the subtropical gyres could be a solution as proposed by
386 (Dutkiewicz et al., 2015) using DARWIN-MITgcm. This has led to an enhancement of lateral nutrients supplies caused
387 by a decrease of productivity in high latitude. Furthermore, skill assessment of 21 regional and global coupled
388 biogeochemical models based on functional group approach including (PISCES, PlankTOM, COBALT, TOPAZ,
389 HAMOCC, BIOMASS, MEDUSA, ERSEM, PELAGOS, PISCES, NOBM) were conducted for the Arctic region
390 studies in order to investigate the capability of these models in representing the observed nitrate, mixed layer depth,
391 as well as euphotic layer depth. Most of the models have shown positive bias for the depth averaged nitrate explaining
392 the overestimation of nitrate in the upper layer (r ≤ 0.68) and none of these models were able to well represent the

https://doi.org/10.5194/bg-2021-351
Preprint. Discussion started: 24 January 2022

variability in the field measurements. However, REcoM is applied and has shown to have a good performance for DIN and silicate (r = 0.75) when coupled to a high resolution setup in the Arctic regions (Schourup-Kristensen et al., 2018).

3.3 Micronutrients (Fe)

Low iron concentrations were simulated in the North and North Central Pacific, North Atlantic, and Antarctic whereas in the North and Equatorial Indian and North Central Atlantic high levels were predicted using NOBM. The overestimation has resulted in r ~ 0.86 and the reason of the iron overprediction is attributed to the lack of scavenging, excessive remineralization, and slow detritus sinking rate. However, PISCES-NEMO has shown a significant underestimation for the spatial variability of iron in the global ocean with r = 0.75 suggesting a need to increase or make the sediment source of iron highly variable since it is too small in the model (Aumont et al., 2015). It is also suggested that iron supply to the surface layer is highly driven by eddies using a simplified version of DARWIN biogeochemical model of two species as described in (Dutkiewicz et al., 2009) coupled to a flat bottom zonally re-entrant MITgcm model (Uchida et al., 2019). So, a better representation of the iron fluxes in the Southern Ocean requires correct energetics of the mesoscale field which can be done by resolving and parametrizing the inverse energy cascade caused by baroclinic instabilities of meso and sub-mesoscale (Person et al., 2019). Hence, (Jiang et al., 2019) applied a modified version of Chai model coupled to ROMS which involved two phytoplankton groups (small phytoplankton and diatoms), two zooplankton groups (micro and meso zooplankton), nutrients (nitrogen, silicate, iron) indicating that dominant iron sources in the Scotia Sea are derived from sediments in the Antarctic Peninsula shelf along with the South Orkney Plateau. In addition to these sources, the Antarctic Circumpolar Current, the northern side of the Weddle Gyre, upwelling, atmospheric dust deposition, and icebergs are the common sources of iron in the Southern Ocean (Jiang et al., 2019). The iron levels estimated by the modified Chai model have shown an average overestimation by 0.26 nM deviated from the observed average value of 0.35 nM resulting in r = 0.76.

3.4 Carbon

Ocean carbon has been derived in different forms including the particulate organic and inorganic carbon (POC, PIC), partial pressure of CO2 (pCO2) and dissolved inorganic carbon (DIC). A representation of the variable POC reactivity evolved from reactive continuum model suggested by (Boudreau and Ruddick, 1991) and was introduced

https://doi.org/10.5194/bg-2021-351
Preprint. Discussion started: 24 January 2022

in PISCES with a coarse resolution NEMO for the global oceans (Aumont et al., 2017). With the POC introduction into the model, the POC levels in the ocean's interior increased by 1 to 2 orders of magnitude which has resulted from the slow sinking of small particles from the surface. In addition, an increase of higher than a factor of 2 of the carbon reaching the sediments has been attained showing better agreement with observations with Root Mean Squared Error (RMSE) of 0.14 (without continuum reactivity), and 0.08 (with continuum reactivity). In addition, PISCES-MITgcm has been used to qualitatively study the carbon cycle in the Arctic Ocean showing the capability in capturing the observed seasonal and regional trends of the dissolved pCO2 (Manizza et al., 2011). However, the spring surface pCO2 in the Canadian Archipelago is underestimated (~300 µatm) relative to observations (400-450 µatm) but able to capture the summer levels (200-250 µatm). The riverine POC and the impact of terrestrial carbon resulted from coastal erosion were neglected in the model hence caused the underprediction of carbon balance. Additionally, the sedimentation and resuspension processes were neglected by the model which may be important in the enrichment of the water column with carbon hence impacting air-sea gas exchange. In addition, the modelled surface DIC by PISCES-NEMO was comparable to observations with r of 0.91 (Aumont et al., 2015). With regard to the comparison conducted between PISCES-NEMO and TOPAZ-NEMO (Jung et al., 2019) for the surface DIC, TOPAZ-NEMO has represented similar agreement with observation ($r > 0.95$), and the zonal averaged surface content is better represented by TOPAZ-NEMO in the Northern Hemisphere (bias < 10 µmol kg^{-1}). Similarly, compared to observations lower bias is shown for surface alkalinity by TOPAZ-NEMO than that of PISCES-NEMO in all oceans (e.g. Southern Hemisphere: negative bias ~ 80 µgmol kg^{-1}, Equator: positive bias, mainly ≤ 16 µmol kg^{-1}, Indian Ocean: negative bias, mainly < 32 µmol kg^{-1}, Pacific: positive bias, mainly ≤ 16 µmol kg^{-1}, Atlantic: negative bias, mainly < 64 µmol kg^{-1})

3.5 Oxygen

Surface oxygen level was estimated in the global oceans by PISCES-NEMO which has resolved the oxygen distribution with r ~ 0.97 because oxygen reach closely to its solubility level and hence is constrained by sea surface temperature (Aumont et al., 2015). Moreover, TOPAZ and PISCES coupled to NEMO (Jung et al., 2019) have shown comparable spatial distributions (r ~0.98) and zonal averages of surface dissolved oxygen (DO) to the observed data for DO in the global oceans but the overall was underestimated by TOPAZ (bias ~ -10 µmol kg^{-1}) and a slight

https://doi.org/10.5194/bg-2021-351
Preprint. Discussion started: 24 January 2022


Biogeosciences Discussions Open Access EGU

448 overprediction of DO (bias ~10 μmol kg^{-1}) was observed by PSICES except in polar regions. Because in polar regions
449 (areas at 60°N or higher) the availability and quality of satellite data is limited.

450 Both models have shown negative bias (~ 25 μmol kg^{-1}) in deep waters which was caused by the weak North Atlantic
451 deep waters represented by the physical model. TOPAZ-NEMO has also shown a better representation of the oxygen
452 minimum zone in the Pacific Ocean. ERSEM coupled to a 1D Princeton/Mellor–Yamada and GOTM physical models
453 respectively were also implemented to study the global oxygen minimum zone. ERSEM-Princeton/Mellor–Yamada
454 lacks horizontal advective processes which could be enhanced through considering the diurnal physical processes
455 while ERSEM-GOTM ignores the episodic intrusion of oxygen within the oxygen minimum zone (Sankar et al., 2018)
456 (Sankar et al., 2018) (Blackford and Burkill, 2002). Thus, the models have shown contradictions between the estimates
457 and climatological seasonal cycles of oxygen at depths which might be attributed to the lack of lateral circulation in
458 the model. Further studies on the oxygen minimum zone in the Arabian Sea were conducted by (Lachkar et al., 2017,
459 2019, 2020) using Fasham model coupled to ROMS indicating that the primary productivity and oxygen minimum
460 zone are highly impacted by monsoon wind intensification with an overall high $r \sim 0.93$ for oxygen (both seasons) in
461 the upper layer. Nevertheless, the model was incapable of resolving the full eddy spectrum because the resolution was
462 overly coarse. The model has considered the nitrogen as a limiting nutrient neglecting iron, phosphate, and silicate
463 which are the major nutrients limiting phytoplankton growth which may have led to amplify the impact of
464 denitrification on the nitrogen budgets in the Arabian Sea (Lachkar et al., 2017) thus overpredicting the oxygen
465 minimum zone.

466

467 **5 Conclusions**
468

469 This review presents the common biogeochemical models applied on various ecosystems of the world's ocean. These
470 models are evaluated through reviewing the studies that have been conducted to estimate biochemical parameters such
471 as chlorophyll-a, nutrients as well as carbon and oxygen components. Therefore, applications of biogeochemical
472 models on different ecosystems have shown different performances depending on the complexity of these ecosystems
473 and the governing equations. PFT's model approach has proven to be a good estimate of surface nutrients such as
474 nitrogen (N), phosphorous (P), and silica (S) in global oceans with $r \geq 0.85$, ≥ 0.9, and ≥ 0.78 with some

https://doi.org/10.5194/bg-2021-351
Preprint. Discussion started: 24 January 2022

475 inconsistencies apparent if coupled with the low-resolution physical component. NPZD models, for example Fasham,
476 are capable of accurately estimating N, P, and oxygen (O) with $R^2 > 0.9$ (for N, P), and > 0.9 (for O) in the Indian and
477 Pacific ecosystems. In contrast, the most effective prediction of iron with r is obtained between 0.7 and 0.86,
478 particularly for models using the functional group approach. In comparison, the reported performance for chlorophyll-
479 a varies between models and r can range from 0.55 to 0.9. These varying reported performances for these
480 biogeochemical parameters are dependent on the features of the ecosystems and reliability of the physical model.
481 Therefore, when developing the biogeochemical model, it is necessary to take into consideration the most appropriate
482 physical models.

483 **6 Author contribution**

484 Kaltham Ismail and Maryam R. Al Shehhi defined the content of the manuscript. Kaltham Ismail prepared the
485 manuscript and Maryam R. Al Shehhi contributed in revisions and improvements.

486 **7 Competing interests**

487 The authors declare no conflict of interest.

488 **8 Acknowledgements**

489 The authors would like to thank Khalifa University for the financial support. This paper is under the project of
490 modelling the biogeochemistry of the Arabian Gulf waters.

491

492

493

494

495

496

497

https://doi.org/10.5194/bg-2021-351
Preprint. Discussion started: 24 January 2022

9 References

Anugerahanti, P., Kerimoglu, O. and Smith, S. L.: Enhancing Ocean Biogeochemical Models With Phytoplankton Variable Composition, Front. Mar. Sci., 8(July), 1–20, doi:10.3389/fmars.2021.675428, 2021.

Aumont, O., Maier-Reimer, E., Blain, S. and Monfray, P.: An ecosystem model of the global ocean including Fe, Si, P colimitations, Global Biogeochem. Cycles, 17(2), n/a-n/a, doi:10.1029/2001gb001745, 2003.

Aumont, O., Ethé, C., Tagliabue, A., Bopp, L. and Gehlen, M.: PISCES-v2: an ocean biogeochemical model for carbon and ecosystem studies, Geosci. Model Dev. Discuss., 8(2), 1375–1509, doi:10.5194/gmdd-8-1375-2015, 2015.

Aumont, O., Van Hulten, M., Roy-Barman, M., Dutay, J. C., Éthé, C. and Gehlen, M.: Variable reactivity of particulate organic matter in a global ocean biogeochemical model, Biogeosciences, 14(9), 2321–2341, doi:10.5194/bg-14-2321-2017, 2017.

Bacastow, R. and Maier-Reimer, E.: Ocean-circulation model of the carbon cycle, Clim. Dyn., 4(1990), 95–125, 1990.

Baretta-Bekker, J. G., Baretta, J. W. and Ebenhöh, W.: Microbial dynamics in the marine ecosystem model ERSEM II with decoupled carbon assimilation and nutrient uptake, J. Sea Res., 38(3–4), 195–211, doi:10.1016/S1385-1101(97)00052-X, 1997.

Baretta, J. W., Ebenhöh, W. and Ruardij, P.: The European regional seas ecosystem model, a complex marine ecosystem model, Netherlands J. Sea Res., 33(3–4), 233–246, doi:10.1016/0077-7579(95)90047-0, 1995.

Blackford, J. C. and Burkill, P. H.: Planktonic community structure and carbon cycling in the Arabian Sea as a result of monsoonal forcing: The application of a generic model, J. Mar. Syst., 36(3–4), 239–267, doi:10.1016/S0924-7963(02)00182-3, 2002.

Blackford, J. C., Allen, J. I. and Gilbert, F. J.: Ecosystem dynamics at six contrasting sites: A generic modelling study, J. Mar. Syst., 52(1–4), 191–215, doi:10.1016/j.jmarsys.2004.02.004, 2004.

Bonachela, J. A., Klausmeier, C., Edwards, K. F. and Litchman, E.: The role of phytoplankton diversity in the emergent oceanic stoichiometry, , (April 2016), doi:10.1093/plankt/fbv087, 2015.

Boudreau, B. P. and Ruddick, B. R.: On a reactive continuum representation of organic matter diagenesis, Am. J. Sci., 291(5), 507–538, doi:10.2475/ajs.291.5.507, 1991.

Bronselaer, B., Russell, J. L., Winton, M., Williams, N. L., Key, R. M., Dunne, J. P., Feely, R. A., Johnson, K. S. and Sarmiento, J. L.: Importance of wind and meltwater for observed chemical and physical changes in the Southern Ocean, Nat. Geosci., 13(1), 35–42, doi:10.1038/s41561-019-0502-8, 2020.

Buitenhuis, E. T., Hashioka, T. and Quéré, C. Le: Combined constraints on global ocean primary production using observations and models, Global Biogeochem. Cycles, 27(3), 847–858, doi:10.1002/gbc.20074, 2013.

https://doi.org/10.5194/bg-2021-351
Preprint. Discussion started: 24 January 2022

529 Castro de la Guardia, L., Garcia-Quintana, Y., Claret, M., Hu, X., Galbraith, E. D. and Myers, P. G.: Assessing the
530 Role of High-Frequency Winds and Sea Ice Loss on Arctic Phytoplankton Blooms in an Ice-Ocean-Biogeochemical
531 Model, J. Geophys. Res. Biogeosciences, 124(9), 2728–2750, doi:10.1029/2018JG004869, 2019.

532 Cavan, E. L., Henson, S. A., Belcher, A. and Sanders, R.: Role of zooplankton in determining the efficiency of the
533 biological carbon pump, Biogeosciences, 14(1), 177–186, doi:10.5194/bg-14-177-2017, 2017.

534 Chai, F., Lindley, S. T. and Barber, R. T.: Origin and maintenance of a high nitrate condition in the equatorial Pacific,
535 Deep. Res. Part II Top. Stud. Oceanogr., 43(4–6), 1031–1064, doi:10.1016/0967-0645(96)00029-X, 1996.

536 Cherif, M. and Loreau, M.: Towards a more biologically realistic use of Droop ' s equations to model growth under
537 multiple nutrient limitation, , (January), 897–907, doi:10.1111/j.1600-0706.2010.18397.x, 2010.

538 Cox, P. M., Betts, R. A., Jones, C. D., Spall, S. A. and Tollerdell, I. J.: Erratum: Accelaration of global warming due
539 to carbon-cycle feedback in a coupled climate model (Nature (2000) 408 (184-187)), Nature, 408(6813), 750,
540 doi:10.1038/35047138, 2000.

541 Das, D., Chakrabarty, M., Goswami, S., Basu, D. and Chaudhuri, S.: Impact of intra-seasonal oscillations of Indian
542 summer monsoon on biogeochemical constituents of North Indian Ocean, Theor. Appl. Climatol., 136(3–4), 839–848,
543 doi:10.1007/s00704-018-2518-1, 2019.

544 Droop, M. R.: Some thoughts on nutrient limitation in algae, , 264–272, 1973.

545 Droop, M. R.: 25 Years of Algal Growth Kinetics A Personal View, Bot. Mar., XXVI, 99–112, 1983.

546 Druon, J. N., Mannino, A., Signorini, S., McClain, C., Friedrichs, M., Wilkin, J. and Fennel, K.: Modeling the
547 dynamics and export of dissolved organic matter in the Northeastern U.S. continental shelf, Estuar. Coast. Shelf Sci.,
548 88(4), 488–507, doi:10.1016/j.ecss.2010.05.010, 2010.

549 Dugdale, R. C.: Limitation in the Sea : Dynamics , Limnol. Oceanogr., 685–695, 1967.

550 Dunne, J., Gnanadesikan, A., Sarmiento, J. L. and Slater, R. D.: Technical description of the prototype version (v0)
551 of Tracers Of Phytoplankton with Allometric Zooplankton (TOPAZ) ocean biogeochemical model as used in the
552 Princeton IFMIP* model, Biogeosciences Suppl., 7(1), 3593, doi:10.5194/bg-7-3593-2010, 2010.

553 Dutkiewicz, S., Follows, M. J. and Bragg, J. G.: Modeling the coupling of ocean ecology and biogeochemistry, Global
554 Biogeochem. Cycles, 23(4), 1–15, doi:10.1029/2008GB003405, 2009.

555 Dutkiewicz, S., Hickman, A. E., Jahn, O., Gregg, W. W., Mouw, C. B. and Follows, M. J.: Capturing optically
556 important constituents and properties in a marine biogeochemical and ecosystem model, Biogeosciences, 12(14),
557 4447–4481, doi:10.5194/bg-12-4447-2015, 2015.

558 Dutkiewicz, S., Baird, M. and Chai, F.: Synergy between Ocean Colour and Biogeochemical/Ecosystem Models.,
559 2020.

https://doi.org/10.5194/bg-2021-351
Preprint. Discussion started: 24 January 2022

560 Evans, G. T., Parslow, J. S., Evans, G. T. and Parslow, J. S.: A model of annual plankton cycles, Deep Sea Res. Part
561 B. Oceanogr. Lit. Rev., 32(9), 759, doi:10.1016/0198-0254(85)92902-4, 1985.

562 Fasham, M. J. R., Ducklow, H. W. and McKelvie, S. M.: A nitrogen-based model of plankton dynamics in the oceanic
563 mixed layer, J. Mar. Res., 48(3), 591–639, doi:10.1357/002224090784984678, 1990.

564 Fasham, M. J. R., Sarmiento, J. L., Slater, R. D., Ducklow, H. W. and Williams, R.: ECOSYSTEM BEHAVIOR AT
565 BERMUDA STATION "S" AND OCEAN WEATHER STATION "INDIA": A GENERAL CIRCULATION
566 MODEL AND OBSERVATIONAL ANALYSIS, , 7(2), 379–415, 1993.

567 Fennel, K., Spitz, Y. H., Letelier, R. M., Abbott, M. R. and Karl, D. M.: A deterministic model for N2 fixation at stn.
568 ALOHA in the subtropical North Pacific Ocean, Deep. Res. Part II Top. Stud. Oceanogr., 49(1–3), 149–174,
569 doi:10.1016/S0967-0645(01)00098-4, 2001.

570 Fennel, K., Wilkin, J., Levin, J., Moisan, J., O'Reilly, J. and Haidvogel, D.: Nitrogen cycling in the Middle Atlantic
571 Bight: Results from a three-dimensional model and implications for the North Atlantic nitrogen budget, Global
572 Biogeochem. Cycles, 20(3), doi:10.1029/2005GB002456, 2006.

573 Fennel, K., Wilkin, J., Previdi, M. and Najjar, R.: Denitrification effects on air-sea CO2 flux in the coastal ocean:
574 Simulations for the northwest North Atlantic, Geophys. Res. Lett., 35(24), doi:10.1029/2008GL036147, 2008.

575 Follows, M. J., Dutkiewicz, S., Grant, S. and Chisholm, S. W.: Emergent biogeography of microbial communities in
576 a model ocean, Science (80-.)., 315(5820), 1843–1846, doi:10.1126/science.1138544, 2007.

577 Fouest, V. Le, Zakardjian, B., Saucier, F. J. and Starr, M.: Seasonal versus synoptic variability in planktonic
578 production in a high-latitude marginal sea : The Gulf of St . Lawrence (Canada), , 110, 1–21,
579 doi:10.1029/2004JC002423, 2005.

580 Franks P: NPZ Models Of Plankton Dynamics: Their construction,coupling with physics, and application, J.
581 Oceanogr., 58, 379–387, 2002.

582 Friedrichs, M. A. M., Dusenberry, J. A., Anderson, L. A., Armstrong, R. A., Chai, F., Christian, J. R., Doney, S. C.,
583 Dunne, J., Fujii, M., Hood, R., McGillicuddy, D. J., Moore, J. K., Schartau, M., Spitz, Y. H. and Wiggert, J. D.:
584 Assessment of skill and portability in regional marine biogeochemical models: Role of multiple planktonic groups, J.
585 Geophys. Res. Ocean., 112(8), doi:10.1029/2006JC003852, 2007.

586 Galbraith, E. D., Gnanadesikan, A., Dunne, J. P. and Hiscock, M. R.: Regional impacts of iron-light colimitation in a
587 global biogeochemical model, Biogeosciences Discuss., 6(4), 7517–7564, doi:10.5194/bgd-6-7517-2009, 2009.

588 Geider, R. J., MacIntyre, H. L. and Kana, T. M.: A dynamic regulatory model of phytoplanktonic acclimation to light,
589 nutrients, and temperature, Limnol. Oceanogr., 43(4), 679–694, doi:10.4319/lo.1998.43.4.0679, 1998.

590 Gregg, W. W.: A Coupled Ocean General Circulation , Biogeochemical , and Radiative Model of the Global Oceans :
591 Seasonal Distributions of Ocean Chlorophyll and Nutrients, , (September), 2000.

https://doi.org/10.5194/bg-2021-351
Preprint. Discussion started: 24 January 2022

592 Gregg, W. W.: Tracking the SeaWiFS record with a coupled physical/biogeochemical/radiative model of the global
593 oceans, Deep. Res. Part II Top. Stud. Oceanogr., 49(1–3), 81–105, doi:10.1016/S0967-0645(01)00095-9, 2001.

594 Gregg, W. W. and Casey, N. W.: Modeling coccolithophores in the global oceans, Deep. Res. Part II Top. Stud.
595 Oceanogr., 54(5–7), 447–477, doi:10.1016/j.dsr2.2006.12.007, 2007.

596 Gregg, W. W., Ginoux, P., Schopf, P. S. and Casey, N. W.: Phytoplankton and iron: Validation of a global three-
597 dimensional ocean biogeochemical model, Deep. Res. Part II Top. Stud. Oceanogr., 50(22–26), 3143–3169,
598 doi:10.1016/j.dsr2.2003.07.013, 2003.

599 Gregg, W. W., Casey, N. W., O'Reilly, J. E. and Esaias, and W. E.: An Empirical Approach to Ocean Color Data :
600 Reducing Bias and the Need for Post-Launch Radiometric Re- Calibration Accepted for Publication Remote Sensing
601 of Environment 2009 Abstract, Remote Sens. Environ., 113, 1598–1612, 2009.

602 Hauck, J. and Völker, C.: Rising atmospheric CO 2 leads to large impact of biology on Southern Ocean CO 2 uptake
603 via changes of the Revelle factor, Geophys. Res. Lett., 42, 1459–1464, doi:10.1002/2015GL063070, 2015.

604 Heinze, C. and Gehlen, M.: Modeling ocean biogeochemical processes and the resulting tracer distributions, 2nd ed.,
605 Elsevier Ltd., 2013.

606 Heinze, C. and Maier-Reimer, E.: GLACIAL pCO2 REDUCTION, Paleoceanography, 6(4), 395–430, 1991.

607 Hinckley, S., Coyle, K. O., Gibson, G., Hermann, A. J. and Dobbins, E. L.: A biophysical NPZ model with iron for
608 the Gulf of Alaska: Reproducing the differences between an oceanic HNLC ecosystem and a classical northern
609 temperate shelf ecosystem, Deep. Res. Part II Top. Stud. Oceanogr., 56(24), 2520–2536,
610 doi:10.1016/j.dsr2.2009.03.003, 2009.

611 HOLLING CS: The components of predation as revealed by a study of small-mammal predation of the European pine
612 sawfly, Can Entomol 91, 71(547), 293–320, doi:10.2351/1.5058368, 1959.

613 Hood, R. R., Kohler, K. E., McCreary, J. P. and Smith, S. L.: A four-dimensional validation of a coupled physical-
614 biological model of the Arabian Sea, Deep. Res. Part II Top. Stud. Oceanogr., 50(22–26), 2917–2945,
615 doi:10.1016/j.dsr2.2003.07.004, 2003.

616 Hood, R. R., Laws, E. A., Armstrong, R. A., Bates, N. R., Brown, C. W., Carlson, C. A., Chai, F., Doney, S. C.,
617 Falkowski, G., Feely, R. A., Friedrichs, M. A. M., Landry, M. R., Moore, J. K., Nelson, D. M., Richardson, T. L.,
618 Salihoglu, B., Schartau, M., Toole, D. A. and Wiggert, J. D.: Pelagic functional group modeling : Progress , challenges
619 and prospects, , 53, 459–512, doi:10.1016/j.dsr2.2006.01.025, 2006.

620 Jiang, M., Measures, C. I., Barbeau, K. A., Charette, M. A., Gille, S. T., Hatta, M., Kahru, M., Mitchell, B. G., Naveira
621 Garabato, A. C., Reiss, C., Selph, K. and Zhou, M.: Fe sources and transport from the Antarctic Peninsula shelf to the
622 southern Scotia Sea, Deep. Res. Part I Oceanogr. Res. Pap., 150(June), 103060, doi:10.1016/j.dsr.2019.06.006, 2019.

623 Jung, H. C., Moon, B. K., Wie, J., Park, H. S., Lee, J. and Byun, Y. H.: A single-column ocean biogeochemistry model

https://doi.org/10.5194/bg-2021-351
Preprint. Discussion started: 24 January 2022

(GOTM-TOPAZ) version 1.0, Geosci. Model Dev., 12(2), 699–722, doi:10.5194/gmd-12-699-2019, 2019a.

Jung, H. C., Moon, B. K., Lee, H., Choi, J. H., Kim, H. K., Park, J. Y., Byun, Y. H., Lim, Y. J. and Lee, J.: Development and Assessment of NEMO(v3.6)-TOPAZ(v2), a Coupled Global Ocean Biogeochemistry Model, Asia-Pacific J. Atmos. Sci., 411–428, doi:10.1007/s13143-019-00147-4, 2019b.

Kearney, K., Hermann, A., Cheng, W., Ortiz, I. and Aydin, K.: A coupled pelagic-benthic-sympagic biogeochemical model for the Bering Sea: documentation and validation of the BESTNPZ model (v2019.08.23) within a high-resolution regional ocean model, Geosci. Model Dev., 13(2), 597–650, doi:10.5194/gmd-13-597-2020, 2020.

Koné, V., Aumont, O., Lévy, M. and Resplandy, L.: Physical and biogeochemical controls of the phytoplankton seasonal cycle in the Indian Ocean: A modeling study, Geophys. Monogr. Ser., 185, 147–166, doi:10.1029/2008GM000700, 2009.

Kriest, I., Khatiwala, S. and Oschlies, A.: Towards an assessment of simple global marine biogeochemical models of different complexity, Prog. Oceanogr., 86(3–4), 337–360, doi:10.1016/j.pocean.2010.05.002, 2010.

Kwiatkowski, L., Yool, A., Allen, J. I., Anderson, T. R., Barciela, R., Buitenhuis, E. T., Butenschön, M., Enright, C., Halloran, P. R., Le Quéré, C., De Mora, L., Racault, M. F., Sinha, B., Totterdell, I. J. and Cox, P. M.: IMarNet: An ocean biogeochemistry model intercomparison project within a common physical ocean modelling framework, Biogeosciences, 11(24), 7291–7304, doi:10.5194/bg-11-7291-2014, 2014.

Lachkar, Z., Smith, S., Lévy, M. and Pauluis, O.: Eddies reduce denitrification and compress habitats in the Arabian Sea, Geophys. Res. Lett., 43(17), 9148–9156, doi:10.1002/2016GL069876, 2016.

Lachkar, Z., Lévy, M. and Smith, S.: Intensification and deepening of the Arabian Sea Oxygen Minimum Zone in response to increase in Indian monsoon wind intensity, Biogeosciences Discuss., (May), 1–34, doi:10.5194/bg-2017-146, 2017.

Lachkar, Z., Lévy, M. and Smith, K. S.: Strong Intensification of the Arabian Sea Oxygen Minimum Zone in Response to Arabian Gulf Warming, Geophys. Res. Lett., 46(10), 5420–5429, doi:10.1029/2018GL081631, 2019.

Lachkar, Z., Mehari, M., Azhar, M. Al, Lévy, M. and Smith, S.: Fast local warming of sea-surface is the main factor of recent deoxygenation in the Arabian Sea, , (September), 1–27, 2020.

Leles, S. G., Valentin, J. L. and Figueiredo, G. M.: Evaluation of the complexity and performance of marine planktonic trophic models, An. Acad. Bras. Cienc., 88(3), 1971–1991, doi:10.1590/0001-3765201620150588, 2016.

Leonard, C. L., McClain, C. R., Murtugudde, R., Hofmann, E. E. and Harding, L. W.: An iron-based ecosystem model of the central equatorial Pacific, J. Geophys. Res. Ocean., 104(C1), 1325–1341, doi:10.1029/1998jc900049, 1999.

Lo, S., Dutkiewicz, S., Losch, M., Oelker, J., Soppa, M., Trimborn, S., Xi, H. and Bracher, A.: On modeling the Southern Ocean Phytoplankton Functional Types, Biogeosciences Discuss., (July), 1–37, doi:10.5194/bg-2019-289, 2019.

https://doi.org/10.5194/bg-2021-351
Preprint. Discussion started: 24 January 2022

656 Losch, M., Strass, V., Cisewski, B., Klaas, C. and Bellerby, R. G. J.: Ocean state estimation from hydrography and
657 velocity observations during EIFEX with a regional biogeochemical ocean circulation model, J. Mar. Syst., 129, 437–
658 451, doi:10.1016/j.jmarsys.2013.09.003, 2014.

659 Maier-Reimer, E.: GEOCHEMICAL CYCLES CIRCULATION MODEL. D I STR I BUT IONS IN AN OCEAN
660 PREINDUSTRIAL GENERAL TRACER, Meteorologie, 7(3), 645–677, 1993.

661 Maier-Reimer, E. and Hasselmann, K.: Transport and storage of CO2 in the ocean ——an inorganic ocean-circulation
662 carbon cycle model, Clim. Dyn., 2(2), 63–90, doi:10.1007/BF01054491, 1987.

663 Manizza, M., Follows, M. J., Dutkiewicz, S., Menemenlis, D., Mcclelland, J. W., Hill, C. N., Peterson, B. J. and Key,
664 R. M.: A model of the Arctic Ocean carbon cycle, , 116(January), 1–19, doi:10.1029/2011JC006998, 2011.

665 McCreary Jr, J. P., Kohler, K. E., Hood, R. R. and Olson, D. B.: A four-component ecosystem model of biological
666 activity in the Arabian Sea, Prog. Oceanogr., 37(3–4), 193–240, 1996.

667 Mccreary, P., Kohler, K. E., Hood, P., John, S., Albert, K. and Fischer, S.: Mixed-Layer and Biological Variability in
668 the Central, , 106(2000), 7139–7155, 2001.

669 McGillicuddy, D. J., McCarthy, J. J. and Robinson, A. R.: Coupled physical and biological modeling of the spring
670 bloom in the North Atlantic (I): model formulation and one dimensional bloom processes, Deep. Res. Part I, 42(8),
671 1313–1357, doi:10.1016/0967-0637(95)00034-4, 1995.

672 Moore, J. K., Doney, S. C. and Lindsay, K.: Upper ocean ecosystem dynamics and iron cycling in a global three-
673 dimensional model, Global Biogeochem. Cycles, 18(4), 1–21, doi:10.1029/2004GB002220, 2004.

674 Palmer, J. R. and Totterdell, I. J.: Production and export in a global ocean ecosystem model, Deep. Res. Part I
675 Oceanogr. Res. Pap., 48(5), 1169–1198, doi:10.1016/S0967-0637(00)00080-7, 2001.

676 Pant, V., Moher, J. and Seelanki, V.: Multi-decadal variations in the oceanic CO2 uptake and biogeochemical
677 parameters over the northern and southern high latitudes, Polar Sci., 18(March 2018), 102–112,
678 doi:10.1016/j.polar.2018.05.008, 2018.

679 Pauer, J. J., DePetro, P. A., Anstead, A. M. and Lehrter, J. C.: Application of a one-dimensional model to explore the
680 drivers and lability of carbon in the northern Gulf of Mexico, Ecol. Modell., 294, 59–70,
681 doi:10.1016/j.ecolmodel.2014.09.007, 2014.

682 Person, R., Aumont, O., Madec, G., Vancoppenolle, M., Bopp, L. and Merino, N.: Sensitivity of ocean
683 biogeochemistry to the iron supply from the Antarctic Ice Sheet explored with a biogeochemical model,
684 Biogeosciences, 16(18), 3583–3603, doi:10.5194/bg-16-3583-2019, 2019.

685 Le Quéré, C., Sciences, G., Sciences, E., Vi, P., Jussieu, P., Villefranche, O., Cedex, V., Sciences, B., Co, C., Research,
686 M., Handelshafen, A., Sciences, E., Anglia, E., Nr, N., Scotia, N. and Centre, O. S.: Ecosystem dynamics based on
687 plankton functional types for global ocean biogeochemistry models, Glob. Chang. Biol., (2005), 2016–2040,

688 doi:10.1111/j.1365-2486.2005.01004.x, 2005.

689 Le Quéré, C., Buitenhuis, E. T., Moriarty, R., Alvain, S., Aumont, O., Bopp, L., Chollet, S., Enright, C., Franklin, D.
690 J., Geider, R. J., Harrison, S. P., Hirst, A. G., Larsen, S., Legendre, L., Platt, T., Prentice, I. C., Rivkin, R. B., Sailley,
691 S., Sathyendranath, S., Stephens, N., Vogt, M. and Vallina, S. M.: Role of zooplankton dynamics for Southern Ocean
692 phytoplankton biomass and global biogeochemical cycles, Biogeosciences, 13(14), 4111–4133, doi:10.5194/bg-13-
693 4111-2016, 2016.

694 Redfield, A. C.: On the proportions of organic derivatives in sea water and their relation to the composition of
695 plankton, James Johnstone Meml. Vol., (November), 176–192, 1933.

696 Richardson, K. and Bendtsen, J.: Photosynthetic oxygen production in a warmer ocean: The Sargasso Sea as a case
697 study, Philos. Trans. R. Soc. A Math. Phys. Eng. Sci., 375(2102), doi:10.1098/rsta.2016.0329, 2017.

698 Sankar, S., Polimene, L., Marin, L., Menon, N. N., Samuelsen, A., Pastres, R. and Ciavatta, S.: Sensitivity of the
699 simulated Oxygen Minimum Zone to biogeochemical processes at an oligotrophic site in the Arabian Sea, Ecol.
700 Modell., 372(January), 12–23, doi:10.1016/j.ecolmodel.2018.01.016, 2018.

701 Sarmiento, J. L., Fasham, M. J. R., Slater, R. D., Ducklow, H. W. and Williams, R.: A seasonal three-dimensional
702 ecosystem model of nitrogen cycling in the North Atlantic euphotic zone: A comparison of model results with
703 observations from Bermuda Station "S" and OWS "India.," Glob. Biogeochem. Cycles, 7(2), 379, 1993.

704 Schourup-Kristensen, V., Sidorenko, D., Wolf-Gladrow, D. A. and Völker, C.: A skill assessment of the
705 biogeochemical model REcoM2 coupled to the finite element sea-ice ocean model (FESOM 1.3), Geosci. Model Dev.
706 Discuss., 7(4), 4153–4249, doi:10.5194/gmdd-7-4153-2014, 2014.

707 Schourup-Kristensen, V., Wekerle, C., Wolf-Gladrow, D. A. and Völker, C.: Arctic Ocean biogeochemistry in the
708 high resolution FESOM 1.4-REcoM2 model, Prog. Oceanogr., 168(November 2017), 65–81,
709 doi:10.1016/j.pocean.2018.09.006, 2018.

710 Sharada, M. K., Kalyani Devasena, C. and Swathi, P. S.: Iron limitation study in the North Indian Ocean using model
711 simulations, J. Earth Syst. Sci., 129(1), doi:10.1007/s12040-020-1361-9, 2020.

712 Six, K. D. and Maier-Reimer, E.: Effects of plankton dynamics on seasonal carbon fluxes in an ocean general
713 circulation model, , 559–583, 1996.

714 Slagstad, D., Wassmann, P. F. J. and Ellingsen, I.: Physical constrains and productivity in the future Arctic Ocean,
715 Front. Mar. Sci., 2(OCT), doi:10.3389/fmars.2015.00085, 2015.

716 Stock, C. A., Dunne, J. P. and John, J. G.: Drivers of trophic amplification of ocean productivity trends in a changing
717 climate, , 11331–11359, doi:10.5194/bgd-11-11331-2014, 2014a.

718 Stock, C. A., Dunne, J. P. and John, J. G.: Global-scale carbon and energy flows through the marine planktonic food
719 web: An analysis with a coupled physical-biological model, Prog. Oceanogr., 120, 1–28,

720 doi:10.1016/j.pocean.2013.07.001, 2014b.

721 Stock, C. A., Dunne, J. P. and John, J. G.: Progress in Oceanography Global-scale carbon and energy flows through
722 the marine planktonic food web : An analysis with a coupled physical – biological model, Prog. Oceanogr., 120, 1–
723 28, doi:10.1016/j.pocean.2013.07.001, 2014c.

724 Sverdrup, H. U.: On conditions for the vernal blooming of phytoplankton, ICES J. Mar. Sci., 18(3), 287–295,
725 doi:10.1093/icesjms/18.3.287, 1953.

726 Taylor, M. H., Losch, M. and Bracher, A.: On the drivers of phytoplankton blooms in the Antarctic marginal ice zone :
727 A modeling approach, , 118(August 2012), 63–75, doi:10.1029/2012JC008418, 2013.

728 Trull, T. W., Passmore, A., Davies, D. M., Smit, T., Berry, K. and Tilbrook, B.: Distribution of planktonic biogenic
729 carbonate organisms in the Southern Ocean south of Australia: A baseline for ocean acidification impact assessment,
730 Biogeosciences, 15(1), 31–49, doi:10.5194/bg-15-31-2018, 2018.

731 Uchida, T., Balwada, D., Abernathey, R., McKinley, G., Smith, S. and Lévy, M.: The Contribution of Submesoscale
732 over Mesoscale Eddy Iron Transport in the Open Southern Ocean, J. Adv. Model. Earth Syst., 11(12), 3934–3958,
733 doi:10.1029/2019MS001805, 2019.

734 Vichi, M., Pinardi, N. and Masina, S.: A generalized model of pelagic biogeochemistry for the global ocean ecosystem.
735 Part I: Theory, J. Mar. Syst., 64(1–4), 89–109, doi:10.1016/j.jmarsys.2006.03.006, 2007.

736 Ward, B. A., Schartau, M., Oschlies, A., Martin, A. P., Follows, M. J. and Anderson, T. R.: When is a biogeochemical
737 model too complex? Objective model reduction and selection for North Atlantic time-series sites, Prog. Oceanogr.,
738 116, 49–65, doi:10.1016/j.pocean.2013.06.002, 2013.

739 Wassmann, P., Slagstad, D., Riser, C. W. and Reigstad, M.: Modelling the ecosystem dynamics of the Barents Sea
740 including the marginal ice zone: II. Carbon flux and interannual variability, J. Mar. Syst., 59(1–2), 1–24,
741 doi:10.1016/j.jmarsys.2005.05.006, 2006.

742 Wroblewski, J. S., Sarmiento, J. L. and Flierl, G. R.: An Ocean Basin Scale Model of plankton dynamics in the North
743 Atlantic: 1. Solutions For the climatological oceanographic conditions in May, Global Biogeochem. Cycles, 2(3),
744 199–218, doi:10.1029/GB002i003p00199, 1988.

745 Wunsch, C. and Heimbach, P.: Practical global oceanic state estimation, Phys. D Nonlinear Phenom., 230(1–2), 197–
746 208, doi:10.1016/j.physd.2006.09.040, 2007.

747 Xiao, Y. and Friedrichs, M. A. M.: Using biogeochemical data assimilation to assess the relative skill of multiple
748 ecosystem models in the Mid-Atlantic Bight : effects of increasing the complexity of the planktonic food web, , 3015–
749 3030, doi:10.5194/bg-11-3015-2014, 2014.

750 Yool, A., Popova, E. E. and Anderson, T. R.: MEDUSA-1.0: A new intermediate complexity plankton ecosystem
751 model for the global domain, Geosci. Model Dev., 4(2), 381–417, doi:10.5194/gmd-4-381-2011, 2011.

https://doi.org/10.5194/bg-2021-351
Preprint. Discussion started: 24 January 2022

752 Yool, A., Popova, E. E. and Anderson, T. R.: MEDUSA-2.0: an intermediate complexity biogeochemical model of
753 the marine carbon cycle for climate change and ocean acidification studies, Geosci. Model Dev. Discuss., 6(1), 1259–
754 1365, doi:10.5194/gmdd-6-1259-2013, 2013.

755

756

757

758

759

760

761

762

763

764

765

766

767

768

769

770

771

772

773

774

775

776

https://doi.org/10.5194/bg-2021-351
Preprint. Discussion started: 24 January 2022

777 Table 1. Typical functional forms of phytoplankton response to irradiance I. These functional forms can be multiplied
778 by the maximum photosynthesis rate termed as P_{max} in some processes. Adapted from (Franks P, 2002).

Functional Form	Definition
$\frac{I}{I_o}$	Linear response to incident light
$\frac{I}{I_o + I}$	Saturating response
$1 - \exp\left(-\frac{I}{I_o}\right)$	Saturating response
$\tanh\left(-\frac{I}{I_o}\right)$	Saturating response
$\frac{I}{I_o}\exp\left(1 - \frac{I}{I_o}\right)$	Saturating and photo-inhibiting response. I_o represent the maximum photosynthesis rate.

779

780 Table 2. Some of the commonly used functional forms of phytoplankton nutrient uptake. Adapted from (Leles et al.,
781 2016)

Functional Form*	Description
$\frac{V_{max} \cdot N}{k + N}$	Michaelis-Menten/Monod; hyperbolic
$\mu_{max}\frac{1 - \frac{Q_{min}}{Q}}{1 - \frac{Q_{min}}{Q_{max}}}$	Quota Curve; hyperbolic
$\mu_{max}\frac{Q - Q_{min}}{(Q - Q_{min}) + K}$	Quota Curve; rectangular- hyperbolic
$\mu_{max}\frac{(1 + KQ) \cdot (Q - Q_{min})}{(Q - Q_{min}) + KQ \cdot (Q_{max} - Q_{min})}$	Normalized Quota equation; rectangular-hyperbolic

782 * V_{max}: maximum utilization rate of nutrient; k: affinity constant for nutrient uptake; Q_{min}: minimum nutrient quota;
783 Q_{max}: maximum nutrient quota; Q: nutrient quota; K: half saturation constant for quota curve.

784

785

786

787

https://doi.org/10.5194/bg-2021-351
Preprint. Discussion started: 24 January 2022

Table 3. some of the commonly used functional forms of phytoplankton zooplankton grazing. Adapted from: (Leles et al., 2016)

Functional Form*	Description
$\boldsymbol{a \cdot P}$	Holling Type I: linear
$\boldsymbol{\frac{a \cdot P}{1 + a \cdot h \cdot P}}$	Holling Type II: Hyperbolic
$\boldsymbol{\frac{I_{max} \cdot P}{k_1 + P}}$	Michaelis-Menten/Monod Hyperbolic
$\boldsymbol{\frac{a \cdot P^2}{1 + a \cdot h \cdot P^2}}$	Type III: sigmoidal
$\boldsymbol{\frac{I_{max} \cdot P^2}{k_1^2 \cdot P^2}}$	Michaelis-Menten/Monod Sigmoidal
$\boldsymbol{\frac{a_i \cdot P_i}{1 + \sum_1^n a_r \cdot h_r \cdot P_r}}$ **where n is the number of preys**	Type II; hyperbolic. multiple preys
$\boldsymbol{\frac{I_{max} \cdot \sum C_{pi}}{k_1 + \sum C_{pi}}}$ **where** $\boldsymbol{C_{pi} = C_{ri} \cdot P_i}$	Monod; hyperbolic; prey selectivity

*$\boldsymbol{a}$: attack rate; P = phytoplankton availability; h = handling time; $\boldsymbol{I_{max}}$: maximum ingestion rate; $\boldsymbol{k_1}$: half saturation constant for ingestion; i: subscript for prey type; r = subscript relative to prey type weight; $\boldsymbol{C_{pi}}$: potential capture rate; $\boldsymbol{C_{ri}}$: capture rate.

Table 4. Some of the functional forms for mortality rate of both phytoplankton and zooplankton. Adapted from: (Franks P, 2002; Leles et al., 2016)

Functional form of i(P)	Description
$\boldsymbol{m}$	Linear
$\boldsymbol{mP}$	Quadratic non-linear
Functional form of j(Z)	**Description**
$\boldsymbol{m \cdot Z}$	Linear
$\boldsymbol{\frac{m \cdot Z}{k_2 + Z}}$	Hyperbolic
$\boldsymbol{\frac{m \cdot Z^2}{k_2^2 + Z^2}}$	Sigmoidal
$\boldsymbol{\frac{m \cdot Z \cdot c}{k_2 + Z \cdot c}}$	Hyperbolic-intraguild predation

$\boldsymbol{m}$: mortality rate of zooplankton; $\boldsymbol{k_2}$: half satutration constant for zooplankton closure term; $\boldsymbol{c}$: zooplankton fraction foe which closure terms acts.

https://doi.org/10.5194/bg-2021-351
Preprint. Discussion started: 24 January 2022

798 Table 5. Biochemical models applied in the global ocean ecosystems including performance, physical
799 model and model resolution.

Ocean	Model approach	Resolution (grid size)	Key biochemical variables [a]	Physical model	Performance[b]	Ref.
Global	Moore	2-D global grid (100 X 116 grid-points); Longitudinal resolution of 3.6º and variable latitudinal resolution from 1–2º with higher resolution near the equator	Fe	NCAR	Bias: Fe = 265 pM (July-North Pacific) Fe = 14 pM (June-Equatorial Pacific) Fe = 121 pM (May-North Atlantic) Fe = 4514 pM (September/August-Arabian Sea) Fe = 2362 pM (November-Southern Ocean)	(Moore et al., 2001)
Global	NOBM	3-D; 2/3° latitude and 1.25° longitude with 14 layers	Fe, Chl-a	GCM	Fe: r = 0.86 & R^2= 0.74 chl-a: r > 0.7	(Gregg et al., 2003)
Global	HAMOCC5	3-D; horizontal resolution is uniformly 3.5 by 3.5 degrees with 22 vertical layers	Fe, Chl-a	LSG	Bias: Fe = 0.15 nM (at depth of 3000 m) chl-a = 0.24mg/m^3	(Aumont et al., 2003)
Global	ERSEM	1-D water column	Chl-a	GOTM	-	(Blackford et al., 2004)
Global	Moore	3-D 100 X 116 horizontal grid points with a resolution of 3.6º longitude and 0.9º-2º latitude	Fe	CCSM	Refer to Moore et al., 2001	(Moore et al., 2004)
Global	Moore	3-D; 3.6º in longitude; 0.9º– 2º degree in latitude	IC, Fe	NCAR CCSM3	Refer to Moore et al., 2001	(Moore et al., 2006)
Global	Moore	3-D; 3.6° in longitude and 0.8° to 1.8° latitude and 25 levels in the vertical	Fe	CCSM	Refer to Moore et al., 2001	(Moore & Doney, 2007)

https://doi.org/10.5194/bg-2021-351
Preprint. Discussion started: 24 January 2022

Global	PlankTOM	3-D; 2° in longitude, 1.1° average in latitude with 31 vertical levels	Chl-a	NEMO	RSS = -13%	(Buitenhuis et al., 2013)
Global	PISCES	3-D; 2◦ by 2◦cosΦ (where Φ is the latitude) with a focusing of the meridional resolution to 0.5◦ in the equatorial domain. 30 vertical layers	IC, P, N, Fe, Alk, O, S	NEMO	r: C = 0.91 P = ~0.91 N = 0.95 Fe = 0.75 Alk = ~0.8 O = 0.97 S = ~0.85	(Aumont et al., 2015)
Global	DARWIN	3-D; horizontal resolution of 1º x 1º with 23 levels	P, N, S, Chl-a	MITgcm	r: P,N,S > 0.9 Chl-a ~ 0.55	(Dutkiewicz et al., 2015)
Global	PlankTOM	3-D; zonal resolution of 2° and a meridional resolution of 2°×cos(latitude) with 30 z levels	O	NEMO	-	(Andrews et al., 2017)
Global	PISCES	3D; 2◦ by 2◦cos(φ) (where φ is the latitude) with an increased meridional resolution to 0.5◦ in the equatorial domain. 30 vertical layers	POC	NEMO	RMSE: No Reactivity Continuum (RC) = 0.14 With RC = 0.08	(Aumont et al., 2017)
Global	Moore	2-D; horizontal resolution of 0.27°–0.53°	S, N, P, O, DIC flux, Chl-a	NCAR-CSM1	r: S = 0.8 N = 0.95 P = 0.92 O = 0.85 DIC = 0.75 Chl-a = 0.6 (Doney et al., 2009)	(Pant et al., 2018)
Global	Moore	3D; 60 vertical levels, was run at the nominal one-degree resolution	IC & coccolithophores	CESM	Refer to Moore et al., 2001	(Krumhardt et al., 2019)
Global	TOPAZ & PISCES	3-D; horizontal resolution of 2° × 2° (182 × 149 grid points) and meridional resolution of 0.5° with 31 levels	Chl-a, N, P, S, O, IC, Alk	NEMO	r: chl-a :0.6-0.9 (both models) N, P, O, & S, DIC & Alk > 0.95 (Both models)	(Jung et al., 2019a)

https://doi.org/10.5194/bg-2021-351
Preprint. Discussion started: 24 January 2022

Atlantic	Fasham	3-D; 2° horizontal resolution and 25 vertical levels	Chl-a, nutrients	MOM	RMSD = 0.97 (for detrital sinking rate of 10 m d^{-1}) & 0.77 (detrital sinking rate of 1 m d^{-1}) Based on Fasham et al, 1990 metrics	(Oschlies & Garçon, 1999)
Atlantic	Fasham	3-D; horizontal resolution is 10 km, and 30 sigma levels	Chl-a	ROMS	Chl-a Winter: r = 0.75 Spring: r = 0.72 Summer: r = 0.85 Fall: r = 0.83	(Fennel et al., 2008)
Atlantic	Fasham	3-D; 10-km horizontal resolution and 30 terrain-following vertical levels	Chl-a	ROMS	Bias: Chl-a (with DOM) = 4 mgchl/m^3 Chl-a (without DOM) = 6 mgchl/m^3	(Druon et al., 2010)
Atlantic	Fasham	3-D; horizontal resolution of 5 km, and 36 vertical terrain-following layers	Chl-a	ROMS	r: chl-a = Spring: 0.6 Summer: 0.65 Fall: 0.53 Winter: 0.45	(Xue et al., 2013)
Atlantic	ERSEM	3-D; 1/8º horizontal resolution with 43 vertical levels	P, N	OGCM-MED16	r > 0.6	(Lazzari et al., 2016)
Atlantic	ERSEM	3-D; resolution of 1/10º X 1/10º (~10 X10 Km) in the horizontal axis and 24 sigma-levels in the vertical axis	Chl-a, P,N	POM	r: chl-a = 0.64 P = 0.02 mmolP/m^3 N = 0.55 mmolN/m^3	(Kalaroni et al., 2019)
Atlantic	ERSEM	3-D; resolution of 1/10º x 1/10º (~10 X10 Km) in the horizontal axis and 24 sigma-levels in the vertical axis	Chl-a, P	POM	Refer to Kalaroni et al., 2019	(Kalaroni et al., 2020)
Indian	Fasham	3-D; 1º resolution in latitude and longitude with 10 vertical levels	Chl-a, N	OGCM	Bias: Chl-a = 0.1 N = -11 mmolN/m^3	(Ryabchenko et al., 1998)
Indian	ERSEM	1-D; grid size of approximately 20 km with 40 vertical layers	N	Princeton/Mellor –Yamada	Bias: N = 9 mmol/m^3	(Blackford & Burkill, 2002)

https://doi.org/10.5194/bg-2021-351
Preprint. Discussion started: 24 January 2022

Indian	McCreary	1-D; with 4 vertical layers	Chl-a, N	Four-layer model	Bias: Chl-a = 2 mg chl-a/m^3 N = 5 molN/kg	(Hood et al., 2003)
Indian	Fasham	3-D; horizontal resolution of 1/3º both meridionally and zonally with 35 levels	Chl-a, N	MOM	Bias: Chl-a = 0.40 (scale: 0-2 mg/m^3) N = 15 (depth of 75 m) (0-30 mmolN/m^3)	(Kawamiya & Oschlies, 2003)
Indian	PISCES	3-D; mean horizontal resolution of 0.5° by 0.5° cos ϕ (where ϕ is the latitude) with 30 vertical layers	Chl-a	NEMO	-	(Koné et al., 2009)
Indian	PISCES	3-D; resolution 1/12° (~9 km) horizontal grid with 46 vertical layers	Chl-a, Fe	NEMO	Bias: Fe = 0.15 nM (at depth of 3000 m) chl-a = 0.24mg/m^3	(Resplandy et al., 2011)
Indian	McCreary	1-D; 6 vertical layers	Chl-a	Six-layer model	Bias: Chl-a = 2 mgchl-a/m^3	(McCreary et al., 2013)
Indian	Fasham	3-D; 1/12º horizontal resolution with 32 vertical sigma layers	Chl-a, N, O	ROMS	Chl-a: r between 0.69 (summer);0.74(winter) N: r = 0.88 O: r = 0.93	(Lachkar et al., 2017)
Indian	ERSEM	1-D; 100 vertical levels	S, P, N, O	GOTM	r > 0.9 for S,P,N,O	(Sankar et al., 2018)
Indian	Fasham	3-D; horizontal resolution of 1/24º and a vertical grid made of 32 levels	Chl-a, N, O	ROMS	Chl-a: r between 0.69-0.74 N: r = 0.88 O: r = 0.93	(Lachkar et al., 2019)
Indian	PISCES	3-D; grid resolution of 1/10° with 32 vertical layers	Fe	ROMS	Refer to Aumont et al., 2015	(Guieu et al., 2019)
Indian	NOBM	3-D; 1.25° longitude by 2/3° latitude with 14 vertical layers	N, S, Chl-a	OGCM	r: N = 0.9-0.96 S ~ 0.95 Chl-a = 0.78 (in situ) & 0.618 (SeaWiFS)	(Das et al., 2019)

https://doi.org/10.5194/bg-2021-351
Preprint. Discussion started: 24 January 2022

Indian	TOPAZ	3D; 1° horizontal resolution with 1/3° resolution near the equator; 50 vertical layers	Fe	MOM	Bias: Fe = 1.5 nMol/m^3	(Sharada et al., 2020)
Indian	Fasham	3-D; 1/10◦ horizontal resolution with 32 sigma-coordinate vertical layers	Chl-a, N, O	ROMS	r: N & O = 0.9; Chl-a = 0.42 (winter) ,0.67 (fall)	(Lachkar et al., 2020)
Southern	PlankTOM	3-D; 2◦ of longitude and a mean resolution of 1.5◦ of latitude with 30 vertical levels	Chl-a, N, S, P	NEMO	r: Chl-a ~ 0.8(PlankTOM6) Chl-a ~ 0.81(PlankTOM10) P ~ 0.9 (PlankTOM6) P ~ 0.92(PlankTOM10) N ~ 0.9 (PlankTOM6) N ~ 0.85(PlankTOM10) S ~ 0.8(PlankTOM6) S ~ 0.78(PlankTOM10)	(Le Quéré et al., 2016)
Southern	NOBM	3-D; 2/3º latitude and 1 ¼ º longitude with 14 vertical layers	PIC,N, S	OGCM	-	(Trull et al., 2018)
Southern	DARWIN	3D; three horizontal grid spacings are used: 20, 5, and 1 km with 76 vertical layers	Fe	MITgcm	No detailed skill analysis of the biological state variables against observations	(Uchida et al., 2019)
Southern	PISCES	3-D; 1◦ horizontal resolution on an isotropic mercator grid with a local meridional refinement up to 1/3◦ at the Equator with 75 levels	Fe	NEMO	Refer to Aumont et al., 2015	(Person et al., 2019)
Sothern	DARWIN	3-D; with mean horizontal spacing of 18 km and 50 vertical levels	Chl-a	MITgcm	MAE: 0.74 mg chl-a m^{-3}(diatoms) 0.22 mg chl-a m^{-3}(haptophytes)	(Lo et al., 2019)
Southern	Chai	3-D; horizontal scale of 2-3 km with 40 vertical layers	Fe	ROMS	r = 0.76	(Jiang et al., 2019)
Southern	TOPAZ	3-D; 1° × 1° horizontal resolution with increased resolution near the Equator and 50 unevenly spaced vertical levels in depth coordinates	DIC, N	ESM2M	-	(Bronselaer et al., 2020)

https://doi.org/10.5194/bg-2021-351
Preprint. Discussion started: 24 January 2022

Arctic	PISCES	3-D; horizontal resolution with an average spacing of ~ 18 km and 50 levels	DIC	MITgcm	No detailed skill analysis available	(Manizza et al., 2011)
Arctic	21 coupled biogeochemical models with different physical systems [c)]	-	Majority includes N, P, S, Fe	-	r: see below the table [d)]	(Babin et al., 2016)
Arctic	REcoM2	3-D; resolution north of 60°N equals 4.5 km, between 40 and 60°N it is approximately 25 km, while a resolution of nominal 1° is used south of 40°N; 32 vertical levels	DIN, S, Chl-a	FESOM	r: DIN: 0.75 Si:0.75 Chl-a: 0.56 Bias: chl-a ≤ 0.1 mg/m^3; (Schourup-Kristensen et al., 2014)	(Schourup-Kristensen et al., 2018)
Arctic	BLING	3-D; horizontal resolution of 0.25° with 50 vertical levels	Chl-a, DIM	NEMO	R^2: IC ≥ 0.93; Chl-a ≥ 0.76 except in BB & HB regions where R^2 = 0.1 & 0.4 respectively; DIM: 0.84, 0.82, 0.93 for BS, LS, BG respectively. Yet R^2 = -0.21 in BB	(Castro de la Guardia et al., 2019)
Arctic	DARWIN	3-D; 18 km of horizontal resolution with 50 vertical levels	DIC	MITgcm	No detailed skill analysis available	(Manizza, 2019)
Pacific	Leonard	1-D vertical ecosystem model; latitudinal resolution of (1/3) ° near the equator	Chl-a	OGCM	r: chl-a = 0.55 & 0.93 if data from June-August 1998 are excluded	(Christian et al., 2001)
Pacific	Chai	3-D; horizontal resolution of 1/8 degree with 30 levels in the vertical direction	Chl-a	ROMS	Bias: Chl-a = 0.18 mg/m^3 (Scale: 0.05-0.4)	(Xiu & Chai, 2011)

https://doi.org/10.5194/bg-2021-351
Preprint. Discussion started: 24 January 2022

Pacific	Fasham	3-D; 3 km horizontal grid size with 30 vertical levels	N, P	ROMS	RMSD = 0.97 (for detrital sinking rate of 10 m d^{-1}) & 0.77 (detrital sinking rate of 1 m d^{-1}) based on (Fasham et al., 1990)	(Gan et al., 2014)
Pacific	Fasham	3-D; (1/12) ° × (1/12) ° of horizontal resolution, 5 d of temporal resolution and 22 sigma levels	O, N	ROMS	R^2: O = 0.88 N = 0.95	(Ji et al., 2017)
Pacific	PISCES	3D; resolution of 7.5 km and 32 sigma levels	Chl-a, Fe	ROMS	Bias: Chl-a = 12 mg/m^3 Fe = 2.5 nM	(Vergara et al., 2017)
Pacific	TOPAZ	1-D; single water column	Chl-a, O, N, P, S, CO_2	GOTM	r: chl-a = 0.53 O = 0.47 N = 0.31 P = 0.16 S = 0.19 CO_2 = 0.94	(Jung et al., 2019b)
Pacific	Chai	1D; 100 layers in the vertical direction	Chl-a	ROMS	r > 0.6	(Ma et al., 2019)
Pacific	Fasham	3-D; horizontal resolution ranged from ~7 km in the north to ~10 km in the south with respect to a cylindrical map projection with 30 vertical levels	P & N	ROMS	R^2 > 0.9	(Lu et al., 2020)
Pacific	Kearney	3-D; 10km horizontal resolution with 30 depth levels	Chl-a	Bering 10K ROMS	No detailed skill analysis of the biological state variables against observations	(Kearney et al., 2020)

[a]) **N**: nitrogen (NO_3, NH_4); **P**: phosphorus; **S**: silicon; **C**: carbon; **O**: oxygen; **Chl**: chlorophyll; **DIC**: dissolved inorganic carbon; **PIC**: particulate inorganic carbon; **DIN**: dissolved inorganic nitrogen; **DIC**: dissolved inorganic carbon; **POC**: particulate organic carbon; **Alk**: Alkalinity; **TP**: total phosphorous; **TN**: total nitrogen; **NO**x: nitrate+nitrite; **DO**: dissolved oxygen.

[b]) **r**: Pearson correlation coefficient**; R^2**: coefficient of determination**; SCC** = Spearman correlation coefficients**; RSS**: residual sum of squares**; RMSD/E**: root mean square difference/error; **MAE**: mean absolute error.

[c]) 1. NEMO-PISCES; 2.NEMO-PlankTOM5.3; 3.NEMO-PlankTOM10; 4.MOM-COBALT; 5.MOM-TOPAZ; 6.MICOM-HAMOCC; 7.POP-BIOMASS; 8.NEMO-MEDUSA; 9.NEMO-ERSEM; 10.NEMO-updated configuration of ERSEM; 11.PELAGOS(NEMO-BFM); 12.POP-Moore; 13.NEMO-PISCES; 14.NEMO-PISCES; 15.NEMO-PISCES; 16.NorESM(HAMOCC); 17. GISS-E2-R-CC(NOBM); 18.MPI-OM HAMOCC.

[d]) 0.46; -0.01; 0.28; 0.68; 0.66; -0.02; 0.05; 0.49; 0.27; 0.28; 0.57; 0.30; 0.46; 0.06; 0.56;

https://doi.org/10.5194/bg-2021-351
Preprint. Discussion started: 24 January 2022

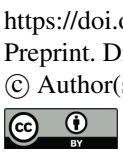

Biogeosciences
Discussions
Open Access
EGU

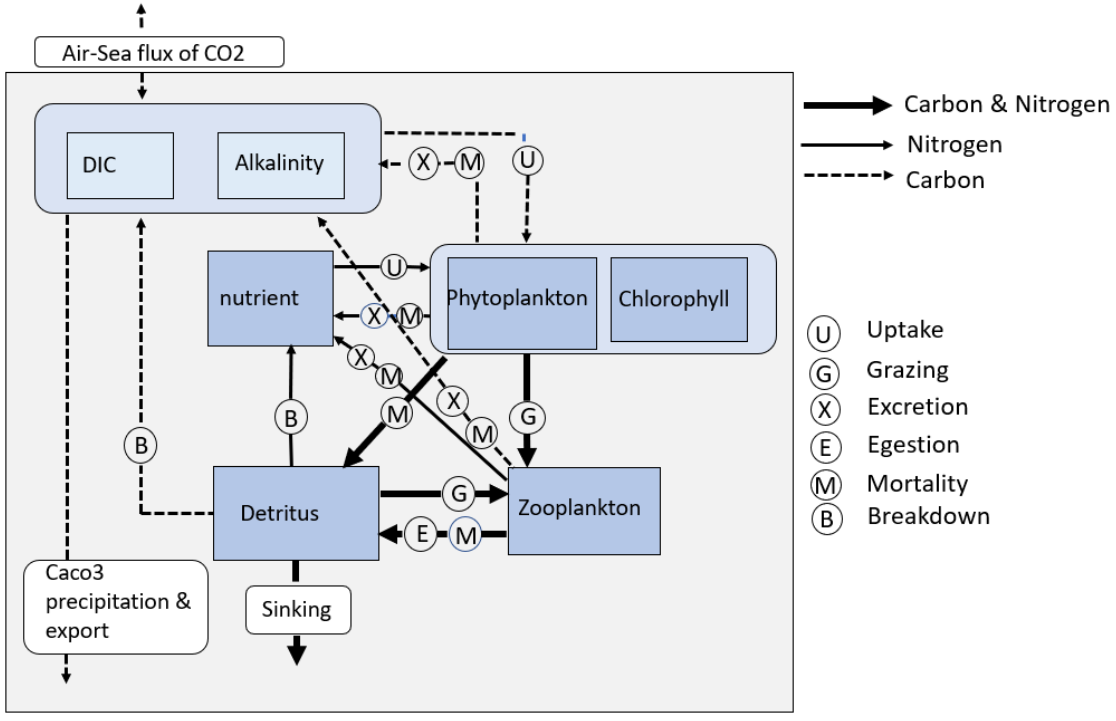

Figure 1. Schematic representation of the Hadley Centre Ocean Carbon model (HadOCC) which is an NPZD model coupled with carbon cycle (Palmer & Totterdell, 2001). The labelled boxes nutrient, phytoplankton, zooplankton, and detritus are representing the